

Re-examining the U.K.'s greatest tornado outbreak: forecasting the limited extent of tornadoes along a cold front

Article

Accepted Version

Apsley, M. L., Mulder, K. J. and Schultz, D. M. (2016) Re-examining the U.K.'s greatest tornado outbreak: forecasting the limited extent of tornadoes along a cold front. *Weather and Forecasting*, 31 (3). pp. 853-875. ISSN 0882-8156 doi: 10.1175/WAF-D-15-0131.1 Available at <https://centaur.reading.ac.uk/61279/>

It is advisable to refer to the publisher's version if you intend to cite from the work. See [Guidance on citing](#).

To link to this article DOI: <http://dx.doi.org/10.1175/WAF-D-15-0131.1>

Publisher: American Meteorological Society

All outputs in CentAUR are protected by Intellectual Property Rights law, including copyright law. Copyright and IPR is retained by the creators or other copyright holders. Terms and conditions for use of this material are defined in the [End User Agreement](#).

www.reading.ac.uk/centaur

CentAUR

Central Archive at the University of Reading

Reading's research outputs online



AMERICAN METEOROLOGICAL SOCIETY

Weather and Forecasting

EARLY ONLINE RELEASE

This is a preliminary PDF of the author-produced manuscript that has been peer-reviewed and accepted for publication. Since it is being posted so soon after acceptance, it has not yet been copyedited, formatted, or processed by AMS Publications. This preliminary version of the manuscript may be downloaded, distributed, and cited, but please be aware that there will be visual differences and possibly some content differences between this version and the final published version.

The DOI for this manuscript is doi: 10.1175/WAF-D-15-0131.1

The final published version of this manuscript will replace the preliminary version at the above DOI once it is available.

If you would like to cite this EOR in a separate work, please use the following full citation:

Apsley, M., K. Mulder, and D. Schultz, 2016: Re-examining the U.K.'s Greatest Tornado Outbreak: Forecasting the Limited Extent of Tornadoes along a Cold Front. *Wea. Forecasting*. doi:10.1175/WAF-D-15-0131.1, in press.

© 2016 American Meteorological Society



1
2
3
4
5
6 **Re-examining the U.K.'s Greatest Tornado Outbreak:**
7 **Forecasting the Limited Extent of Tornadoes**
8 **Along a Cold Front**
9

10
11
12 **MIRIAM L. APSLEY*, KELSEY J. MULDER, AND DAVID M. SCHULTZ**

13
14 *Centre for Atmospheric Science, School of Earth, Atmospheric and Environmental Sciences, University of*
15 *Manchester, United Kingdom*
16

17
18
19
20
21
22 * Additional affiliation: *Christ's College, University of Cambridge, United Kingdom*
23
24
25
26
27
28

29 Submitted as an Article to *Weather and Forecasting* 5 October 2015

30
31 Revised 12 February 2016 and 28 March 2016
32
33
34
35
36
37
38

39 *Corresponding author address:* Prof. David M. Schultz; Centre for Atmospheric Science; School of
40 Earth, Atmospheric and Environmental Sciences; University of Manchester; Simon Building, Oxford
41 Road; Manchester M13 9PL, United Kingdom.
42 E-mail: David.Schultz@manchester.ac.uk

43
44

ABSTRACT

45 On 23 November 1981, a strong cold front swept across the U.K., producing tornadoes from
46 the west to the east coasts. An extensive campaign to collect tornado reports by the Tornado and
47 Storm Research Organisation (TORRO) resulted in 104 reports, the largest U.K. outbreak. The
48 front was simulated with a convection-permitting numerical model down to 200-m horizontal
49 grid spacing to better understand its evolution and meteorological environment. The event was
50 typical of tornadoes in the U.K., with convective available potential energy (CAPE) less than
51 150 J kg^{-1} , 0–1-km wind shear of $10\text{--}20 \text{ m s}^{-1}$, and a narrow cold-frontal rainband forming
52 precipitation cores and gaps. A line of cyclonic absolute vorticity existed along the front, with
53 maxima as large as 0.04 s^{-1} . Some hook-shaped misovortices bore kinematic similarity to
54 supercells. The narrow swath along which the line was tornadic was bounded on the
55 equatorward side by weak vorticity along the line and on the poleward side by zero CAPE,
56 enclosing a region where the environment was otherwise favorable for tornadogenesis. To
57 determine if the 104 tornado reports were plausible, first possible duplicate reports were
58 eliminated, resulting in as few as 58 tornadoes to as many as 90. Second, the number of possible
59 parent misovortices that may have spawned tornadoes is estimated from model output. The
60 number of plausible tornado reports in the 200-m grid-spacing domain was 22 and as many as
61 44, whereas the model simulation was used to estimate 30 possible parent misovortices within
62 this domain. These results suggest that 90 reports was plausible.

63

64 **1. Introduction**

65 On 23 November 1981, a strong cold front swept across the U.K., producing an
66 unprecedented 104 reports of tornadoes (Fig. 1). Called “Britain’s greatest tornado outbreak”
67 (Rowe and Meaden 1985), this event had many more tornadoes than the next largest event just a
68 month earlier on 20 October 1981, which spawned only 29 tornadoes (Turner et al. 1986; Rowe
69 2016). For comparison, even modest outbreaks by United States standards are relatively
70 uncommon in the U.K. Specifically, over 90% of U.K. tornado days between 1980 and 2012 had
71 fewer than 8 tornadoes (Fig. 14 in Mulder and Schultz 2015). The November 1981 outbreak is
72 so exceptional that it distorts the historical record and climatologies of tornadoes in the U.K. and
73 Europe. For example, in the U.K. tornado climatology by Mulder and Schultz (2015), several
74 figures had to be plotted with the outbreak excluded (e.g., their Figs. 5–7, 9, 12, 13), and, in their
75 review of tornadoes across Europe, Antonescu et al. (2016) found that the large number of
76 reports produced a bias in their synthesized results and capped the total number of reports from
77 this outbreak at 58. Given the large number of reports distorting the climatologies and that a
78 scientific study of this event has not been performed in nearly 35 years, we believe that the time
79 is right to re-examine this event.

80 The locations of these 104 reports (Fig. 1) come from the Tornado and Storm Research
81 Organisation (TORRO). TORRO is a U.K. not-for-profit organization responsible for collecting
82 tornado reports from the media, from over 350 observers in the U.K., and from the public
83 through TORRO’s website <http://www.torro.org.uk> (e.g., Elsom et al. 2001; Doe 2016). Of the
84 104 reports on 23 November 1981, 35 came from media reports, 30 came from the public after a
85 call for reports on Anglia Television, and 39 were the result of TORRO’s appeal in local
86 newspapers (Rowe 1985). The challenges of severe-weather event verification can be immense,

87 even when events are well observed by expert meteorologists (Speheger et al. 2002; Trapp et al.
88 2006). The challenges are compounded when reports are collected well after the event from
89 primarily nonmeteorologists, as was the case in this event.

90 The first tornadoes of the day occurred in Anglesey, on the west coast of Wales, where there
91 were five reports around 1000 UTC; 20 houses were damaged there, and a summer house
92 (comparable to a small temporary building or mobile home) was turned upside down (Kemp and
93 Morris 1982). The next seven tornado reports occurred near Aughton (near Liverpool) at 1100
94 UTC, and there were four more in Greater Manchester at 1200 UTC. A further 11 reports in the
95 early afternoon came from Birmingham, Nottinghamshire, and the East Midlands (east of
96 Birmingham), where 20 large caravans (camper vans) were blown over (Rowe and Meaden
97 1985). Seven tornado reports clustered near Hull in the early afternoon. Many of the reports
98 (43), however, came from East Anglia (northeast of Cambridge) between 1300 and 1600 UTC.
99 The last tornadoes occurred in southeast Essex (east-northeast of London) just before 1600 UTC.

100 Despite the large number of reports and despite occurring in conjunction with an extensive
101 southwest–northeast-oriented cold front advancing southeastward across nearly the entirety of
102 the U.K., these tornado reports only occurred along a narrow swath 200–250 km wide and 400
103 km long (Fig. 1). Thus, *the first goal of this article is to determine why the tornadoes occurred in*
104 *a narrow swath along an otherwise extensive cold front.*

105 There are few exact details given with most of the tornado reports, so the duration of each
106 tornado is unknown; some eyewitnesses, however, estimated lifetimes of 20–30 seconds or less
107 (Rowe 1985). Eight tornado reports included damage track lengths between 0.3 and 4 km long.
108 Where estimated, damage tracks are believed to have had widths of 10–20 m. The direction of
109 travel was reported in 16 cases, with 14 coming from between west and north-northwest,

110 consistent with the movement of the front; the other 2 came from the south and southwest.
111 Ninety-nine of the 104 reports were assigned values on the International Tornado Intensity Scale
112 or T scale (Meaden 1983; Meaden et al. 2007). Compared to the Fujita (F) scale, the T scale has
113 twice as many classifications. Conversion between the F and T scales can be performed using the
114 equation $F \approx 0.5T$ and rounding down to the nearest integer (Brooks and Doswell 2001; Meaden
115 et al. 2007). Figure 2 shows that most (96, or 97%) of the tornadoes were T0–T3 (or F0–F1);
116 three tornadoes, however, reached T4 (or F2). This distribution is similar to the national
117 distribution from the Kirk (2014) and Mulder and Schultz (2015) climatologies in which 94–95%
118 were between T0–T3 (or F0–F1).

119 Because tornado reporting in this event relied on responses from a media campaign, the
120 figure of 104 tornado reports has been controversial. Extrapolating based on the density of
121 reports and the sparsely populated areas over which most of the cold front traveled, Rowe and
122 Meaden (1985) suggested that the number of tornadoes may possibly have been as high as 400–
123 500. On the other hand, only 58 of these reports (56% of the 104 reports) were later verified by
124 TORRO experts according to the TORRO database and classified as definite; the other 46 reports
125 were deemed to show reasonable evidence of a tornado having occurred, but not enough to be
126 certain—these were classified as probable. Thus, the lack of confirmation of nearly half of the
127 reports and the extreme magnitude of the outbreak in the historical context suggest that the 104
128 reports might be an overestimate.

129 In this article, we use two different approaches to investigate the tornado reports. First, we
130 undertake a re-examination of the individual tornado reports for the possible occurrence of
131 multiple reports of the same tornado. Second, we use a cloud-resolving model to simulate the
132 cold front and possible parent circulations to the tornadoes. The number of parent circulations

133 might give us some insight into the number of tornadoes. Thus, *the second goal of this article is*
134 *to re-examine the tornado reports and the meteorological conditions on that day to see if we can*
135 *constrain the minimum and maximum number of tornadoes that likely occurred.*

136

137 **2. Background on tornadoes along cold fronts**

138 Tornadoes forming along cold fronts are a challenging forecasting problem. Such tornadoes
139 are often associated with a class of convective storms occurring along cold fronts called narrow
140 cold-frontal rainbands. Narrow cold-frontal rainbands have been described by Browning and
141 Harrold (1970), Browning and Pardoe (1973), Carbone (1982), Hobbs and Persson (1982),
142 Browning and Reynolds (1994), Browning and Roberts (1996), Browning et al. (1997),
143 Jorgensen et al. (2003), and Viale et al. (2013), among many others. Narrow cold-frontal
144 rainbands have been synthesized by conceptual models in Browning (1990) and Houze (2014,
145 section 11.4.4). In the United States, narrow cold-frontal rainbands are a subset of what have
146 been termed *quasi-linear convective storms* (QLCSs; Trapp et al. 2005). Trapp et al. (2005)
147 applied this term for their investigation of tornadoes that form along such line convection (i.e.,
148 distinct from supercell convective storms).

149 Tornadoes along linear convective systems are challenging because they tend to have shorter
150 lead times than tornadoes associated with supercells (Trapp et al. 2005). Even if the specific
151 location and timing of the tornadoes cannot be predicted well in advance, predicting the general
152 location along the line where tornadoes form would be an operationally useful tool. Indeed,
153 Atkins et al. (2004) showed that tornadoes were more likely to form from parent mesovortices
154 along the convective line that had greater rotation rates, implying that the strongest vortices may
155 favor tornadogenesis.

156 Before discussing how tornadoes form along linear convective storms, we need to distinguish
157 between the parent circulations that precede the tornadoes and the tornadoes themselves. One of
158 the characteristics often observed in narrow cold-frontal rainbands is the presence of
159 precipitation cores and gaps, aligned anticyclonically relative to the front. These core-and-gap
160 regions have been reported for cold fronts over the eastern North Pacific Ocean (e.g., Hobbs and
161 Biswas 1979; Hobbs and Persson 1982; Jorgensen et al. 2003), near the Alps (Hagan 1992), over
162 eastern North America and the Atlantic Ocean (Locatelli et al. 1995; Wakimoto and Bosart
163 2000), and over the U.K. (e.g., James and Browning 1979; Browning and Roberts 1996).
164 Specifically, other tornadic cold fronts in the U.K. also possessed this core-and-gap structure
165 (e.g., Smart and Browning 2009; Clark and Parker 2014; Mulder 2015), as well as in Japan (e.g.,
166 Kobayashi et al. 2007; Sugawara and Kobayashi 2009).

167 The cores are often associated with heavier precipitation and relative maxima in vorticity
168 (hereafter misovortices), whereas the gaps are associated with weaker precipitation or the
169 absence of precipitation and relative minima in vorticity. Misovortices have diameters of 1–4
170 km (Fujita 1981) and have been suggested to be the parent circulation from which the tornadoes
171 form. Different explanations have been offered to explain misovortex formation, including the
172 release of horizontal shearing instability (e.g., Carbone 1982; Hobbs and Persson 1982; Lee and
173 Wilhelmson 1997b; Jorgensen et al. 2003; Wheatley and Trapp 2008; Kawashima 2011),
174 advection of hydrometeors (Locatelli et al. 1995), trapped gravity waves (Brown et al. 1999),
175 tilting of vorticity along the cold front (Carbone 1983), or combinations of the above.

176 How tornadoes form along linear convective storms is less well known compared to
177 supercellular tornadoes, primarily because detailed field observations of tornadoes forming along
178 linear convective storms have not been collected and because of the large computational expense

179 of producing a tornado within a numerical model. Because of the shorter lead time and the
180 different parent-storm morphology to supercells, Trapp et al. (1999) suggested that a different
181 tornadogenesis mode may be responsible for tornadoes from linear convective systems than
182 tornadoes from supercells. Carbone (1983) found that the downdraft was coincident with the
183 tornado, suggesting the importance of tilting and a similarity with tornadogenesis in supercells.
184 In contrast, Lee and Wilhelmson (2000) found the importance of stretching of strong initial
185 vorticity in their simulations of nonsupercell tornadogenesis. Nevertheless, the data and
186 simulations in this article will be insufficient to address the issue of tornadogenesis in this case.
187 Thus, we focus on the mesocyclones, the locations of the tornadoes, and an approach to forecast
188 the occurrence of tornadoes along lines, as demonstrated for the case of Britain's greatest
189 tornado outbreak on 23 November 1981.

190

191 **3. Observations: Synoptic and mesoscale overview**

192 At 12 UTC 22 November 1981, archived Met Office charts identified a broad region of low
193 pressure with two centers of 994 hPa and 996 hPa centered southeast of Iceland and north of the
194 U.K. (Fig. 3a). Twelve hours later, the cyclone consolidated with a central pressure of 986 hPa
195 (not shown). By 12 UTC 23 November, the low had rapidly deepened another 18 hPa to 968 hPa
196 and was moving toward Norway (Fig. 3b), making landfall by 0600 UTC 24 November with a
197 central pressure of 959 hPa (not shown). The cyclone was associated with a sharp trough in 500-
198 hPa geopotential height and strong geostrophic cold advection in the lower troposphere, as
199 indicated by the 1000–500-hPa thickness contours (Fig. 4).

200 Associated with this cold advection was a strong cold front at the surface. Archived hourly
201 Met Office surface maps show the front extending to the south of the cyclone across the U.K.

202 and its southeastward progression (Fig. 5). As the cold front crossed England and Wales,
203 temperatures fell by 6–7°C in the first hour, and the pressure rose by as much as 4–5 hPa in the
204 first hour after frontal passage and 3 hPa hr⁻¹ thereafter (Rowe and Meaden 1985; Fig. 5). The
205 wind direction veered suddenly from 190°–230° before the front, a direction roughly parallel to
206 the front, to 320°–340° after the front, a postfrontal direction nearly perpendicular to the
207 orientation of the front (e.g., Fig. 5c). By 1800 UTC, the cold front had cleared England and
208 moved over the North Sea (Rowe 1985; Rowe and Meaden 1985). Moderate rain preceded and
209 was associated with the front in northwestern England at the hour ending 1200 UTC (as much as
210 10 mm per hour; Fig. 6). The infrared satellite image at 1325 UTC (Fig. 7) showed the low
211 center to the north of the U.K. and the broad band of clouds associated with the cold front and a
212 prefrontal band. As the front moved southeastward into central England, the precipitation
213 weakened dramatically to less than 2 mm per hour during the hour ending at 1400 UTC (Fig. 6).

214 Unfortunately, none of the operational soundings that day were ideal for sampling the
215 prefrontal air. The nearest proximity sounding occurred at Aughton near Liverpool, about 11 h
216 before frontal passage at 0000 UTC (Fig. 8). This sounding exhibited only 13 J kg⁻¹ convective
217 available potential energy (CAPE), a steep lapse rate between 850 and 700 hPa, and a strong 60
218 kt (31 m s⁻¹) westerly wind at 850 hPa (Fig. 8). A sounding from the NCEP–NCAR Reanalysis
219 (Kalnay et al. 1996) for a location in western England (52.5°N, 2.5°W) at 1200 UTC 23
220 November had a surface-based CAPE of 147 J kg⁻¹, which is only slightly higher than the 50–
221 100 J kg⁻¹ of CAPE from the model simulation initialized from the European Centre for
222 Medium-Range Weather Forecasting (ECMWF) reanalyses (jump ahead to Fig. 13).

223 These conditions—strong cold front, small CAPE, prefrontal winds nearly parallel to the
224 front, and postfrontal winds nearly perpendicular to the front—are consistent with weather

225 conditions associated with other tornado outbreaks in the U.K. (e.g., Bolton et al. 2003; Holden
226 and Wright 2004; Clark 2009, 2013; Clark and Parker 2014; Mulder 2015). Given the synoptic
227 situation, the morphology of the convective storm (also called its convective mode) is likely
228 consistent with previous tornadic convective storms over the U.K., which tend to occur along
229 cold fronts in linear convective storms. Linear convective storms account for 42% of the
230 tornadoes and 51% of the tornado outbreaks in the U.K. (Mulder and Schultz 2015), unlike in the
231 United States where linear storms account for only 18–25% of the tornadoes (Trapp et al. 2005;
232 Smith et al. 2012). [In comparison, supercells produce 79% of U.S. tornadoes (Trapp et al.
233 2005).] Clark (2013) examined 103 convective lines in the UK and found that 27% were
234 associated with at least one tornado, further evidence for the importance of these lines in
235 producing tornadoes in the U.K.

236 Because radar data for this event (Doppler winds or even reflectivity) are unavailable, the
237 precipitation structure of the cold front on that day is unknown. Therefore, we investigate this
238 event further with a model simulation.

239

240 **4. Model simulation: Set-up**

241 As has been demonstrated for other cases, model simulations can be an effective tool for
242 understanding tornadic fronts in the U.K. (e.g., Smart and Browning 2009; Groenemeijer et al.
243 2011; Mulder 2015). Therefore, we performed a convection-permitting simulation to construct a
244 four-dimensionally consistent dataset to explore a likely meteorological evolution for this event.
245 A successful simulation would be useful to interpret the conditions favorable for the tornadoes
246 within the narrow swath and help interpret the 104 reports of tornadoes.

247 The simulation was performed using the Advanced Research Weather and Forecasting
248 Model version 3.4.1 (WRF-ARW; Skamarock et al. 2008). The simulation was initialized at
249 0600 UTC 23 November 1981 from the ECMWF reanalysis at $0.25^\circ \times 0.25^\circ$ grid spacing
250 interpolated onto a Lambert conformal grid. Lateral boundary conditions were provided by the
251 ECMWF reanalyses every 6 h. Otherwise, the simulation was set up exactly the same as that in
252 Mulder (2015) for the more modest U.K. tornado outbreak of 29 November 2011, which featured
253 seven reported tornadoes across Wales and northern England. The simulation featured 90
254 vertical levels and four domains, ranging from the outermost domain with 25-km horizontal grid
255 spacing, to three two-way nested domains of 5-km, 1-km, and 200-m horizontal grid spacing (the
256 innermost two domains are shown in Fig. 9). Even at 200-m grid spacing, the model would have
257 been inadequate to resolve any possible tornadoes. Instead, the innermost domain is analyzed for
258 the existence of mesocyclones, small-scale circulations along linear convective systems that may
259 precede tornadoes. Only output from the 1-km and 200-m domains is shown in the present
260 article. Model output was saved for further diagnosis every 30 min for the 1-km domain and
261 every 10 s for the 200-m domain.

262 The Kain–Fritsch convective parameterization (Kain and Fritsch 1990; Kain 2004) was
263 employed on the outermost 25-km domain only. Other physical parameterizations included the
264 five-layer thermal diffusion land-surface scheme (Skamarock et al. 2008, their section 8.4.1),
265 Thompson et al. (2008) cloud microphysics, and Mellor–Yamada–Janjić boundary layer (Mellor
266 and Yamada 1982; Janjić 1994, 2002). These parameterizations were chosen because Mulder
267 (2015) found that they produced the most successful simulation of her case. Testing three
268 different microphysical parameterizations (WRF single-moment six-class scheme; Morrison et

269 al. 2009; Thompson et al. 2008) did not produce different structures for the core-and-gap regions
270 along the cold front in this case.

271

272 **5. Model simulation: Mesoscale analysis**

273 The meteorology on the 1-km domain is presented in this section. Subsequent analysis in
274 this article occurs at 1000 UTC, around the time the first tornadoes were reported in Anglesey,
275 and at 1400 UTC, just before the majority of tornadoes were reported in East Anglia. To
276 illustrate the intensity of the front, surface temperature, wind, and sea-level pressure at 1000
277 UTC and 1400 UTC are presented in Fig. 10. The passage of the front was associated with a
278 sharp pressure trough, temperature drop of 6°–8°C, and nearly a 90° veering of the wind (Fig.
279 10). The winds on either side of the front changed direction from 180°–230° on the warm side to
280 310°–330° on the cold side, although the wind speeds were roughly the same across the front at
281 about 5–10 m s⁻¹. The simulation is consistent with the observations reported in section 3,
282 except for the simulation being an hour behind the observations (cf. Figs. 5a and 10a; cf. Figs. 5c
283 and 10b).

284 At 1000 UTC 23 November, simulated radar reflectivity factor reveals poorly organized
285 precipitation along the pressure trough over most of the domain, with reflectivities of up to 45
286 dBZ, ahead of the wind shift along the cold front around the time the band first arrived in the
287 U.K. (Fig. 11a). Along the cold front in the northwest part of the domain, a shorter, narrower,
288 more organized, and more intense (45–50 dBZ) line of convection developed (Fig. 11a). As the
289 rainband progressed across the U.K., the areal coverage of the precipitation decreased as the
290 along-front extent of the rainband increased, consistent with the observations (cf. Figs. 6 and 11).
291 In particular, as the line passed over the Pennine mountain range in the center of northern

292 England, much of the precipitation weakened and the band split into a higher reflectivity line
293 positioned along the front, and a line of precipitation tens of km ahead of the front (Fig. 11b).
294 The observed counterpart to the modeled prefrontal band, although present in the satellite
295 imagery (Fig. 7 at 1325 UTC), did not appear to produce any measurable precipitation at the rain
296 gauges (Fig. 6 during 1300–1400 UTC). Whether this is because the band was poorly forecast or
297 the stations did not receive rain is unclear at this time. In any case, this prefrontal band is not the
298 focus of the article as it is not associated with the formation of the tornadoes. At maturity of the
299 convective line, cores of stronger precipitation became separated by gaps of about 10 km in
300 length of lighter or no precipitation, similar to previously published work summarized in section
301 2.

302 The front was associated with a line of absolute vorticity maxima at 500 m above sea level,
303 which was strongest to the north and weakest to the south (Fig. 12) because the zone of wind
304 shift across the front broadened in association with a weaker pressure trough (Figs. 5b,c and
305 10b). This line of absolute vorticity maxima was between 0.005 and 0.01 s^{-1} and contained small
306 maxima of 0.01–0.02 s^{-1} , as calculated on the 1-km grid. The line of vorticity moved across
307 Britain with the cold front (Fig. 12); there were maxima in vorticity over Anglesey at 1100 UTC,
308 near Liverpool about 1200 UTC, and in southeast England at 1500–1600 UTC, passing southeast
309 of the U.K. by 1730 UTC. These times correspond within about an hour of reported tornado
310 times (Rowe and Meaden 1985), which is all that can be expected given that the resolution of the
311 tornado reports is only hourly, providing additional faith in the ability of the simulation to
312 reproduce observed features of the front.

313 An examination of the three ingredients for deep moist convection (lift, moisture, and
314 instability; e.g., Johns and Doswell 1992) shows that lift as much as several $m s^{-1}$ was present

315 (not shown), associated with the strong convergence along the cold front inferred from the wind
316 field (Fig. 11b). Moisture and instability can be diagnosed by CAPE (determined from the
317 parcel with the maximum equivalent potential temperature in the column) (Fig. 13). At 1000
318 UTC, CAPE appeared as patchy areas east of the front, but generally less than 50 J kg^{-1} (Fig.
319 13a). By 1400 UTC, CAPE increased ahead of the front, with widespread areas over 25 J kg^{-1}
320 and localized maxima approaching 125 J kg^{-1} , forming a slightly curved narrow (40–70 km
321 wide) crescent of CAPE ahead of the front (Fig. 13b). (Interestingly, a second maximum of
322 CAPE of $25\text{--}125 \text{ J kg}^{-1}$ was also present in a 20–50-km wide band about 150 km ahead of the
323 front associated with the prefrontal rainband, although this maximum is not part of this story.)
324 Therefore, the three ingredients for deep moist convection (i.e., instability, lift, moisture) were
325 present along the front.

326 These large gradients in CAPE occurring over such short distances raise issues about the
327 proximity soundings for U.K. tornadoes. Given the large gradients in CAPE occur over
328 distances as small as tens of km, this raises questions about the choice of proximity sounding
329 criteria used in Mulder and Schultz (2015) of 180 km and 3 h. Mulder and Schultz (2015)
330 derived their criteria from previous proximity sounding studies in the United States, specifically
331 Brooks (2009). Indeed, the prefrontal sounding for this outbreak in Fig. 8 does not meet these
332 criteria. Other U.K. soundings on that day were even farther away from the tornadoes. Thus, the
333 large variability in CAPE ahead of the front in this case is consistent with the recommendations
334 for proximity sounding criteria for significant tornadoes in the United States of a range of 40–80
335 km and no more than 2 h (Potvin et al. 2010). Potentially noteworthy is the fact that detailed
336 analysis of CAPE and convective inhibition near supercells in the central United States show
337 variations of hundreds of J kg^{-1} over distances as small as a few km (e.g., Markowski et al.

338 2002). Therefore, perhaps our results of such strong gradients over tens of km should not be too
339 surprising.

340 Given the reasonable timing and structure of the modeled front compared to the
341 observations, we can interrogate the model output to determine the reasons that the tornado
342 reports occurred within a relatively narrow swath along the front. Given the existence of
343 organized deep moist convection, the potential for tornadogenesis can be explored with plots of
344 lifting condensation level (LCL), 0–1-km wind shear, and 0–1-km storm-relative helicity. These
345 are quantities known for their ability to discriminate tornadic from nontornadic storms in the
346 United States (e.g., Rasmussen and Blanchard 1998; Thompson et al. 2003, 2012; Craven and
347 Brooks 2004) and Europe (e.g., Púčik et al. 2015; Mulder and Schultz 2015).

348 At 1000 UTC, the lowest LCL along the front was between 600 and 1000 m (Fig. 14a). By
349 1400 UTC, the LCL had dropped along a similar crescent-shaped spatial distribution of low LCL
350 (200–600 m) in the south with patches less than 200 m, and significantly higher LCL (greater
351 than 2200 m) behind the front and to the north along the front (Fig. 14b). These results are
352 consistent with conditions for tornadoes in the U.K. Specifically, Mulder and Schultz (2015)
353 found that low LCL height was a statistically significant factor in predicting tornado formation in
354 the U.K., with outbreaks having a mean LCL of about 700 m, as opposed to a null set of
355 convective storms with lightning or hail which had an LCL of 900 m. Therefore, we would
356 expect tornadic storms to be found along the line toward the south where the LCL is lower and
357 the CAPE is higher.

358 The vertical shear of the horizontal wind over the surface to 1 km layer (i.e., 0–1-km wind
359 shear) displayed a sharp change in magnitude across the front (Fig. 15). Just ahead of the front
360 in the swath where the tornadoes formed, the shear was 10–20 m s^{-1} , with values over 30 m s^{-1} in

361 the prefrontal rainband (Fig. 15b). Behind the front, the shear was only around 5–10 m s⁻¹.
362 Storm-relative helicity over 0–1 km also showed rather large values ahead of the front (Fig. 16).
363 In the immediate vicinity of the front in the prefrontal environment, 0–1-km storm-relative
364 helicity ranged from zero to several hundred m² s⁻² (Fig. 16).

365 Thus, despite the cold front extending across nearly the entirety of the U.K. (Figs. 5b,c), the
366 narrow swath of tornado reports occurred in what was apparently a sweet spot for the conditions
367 favoring deep moist convection and tornadogenesis along squall lines. Specifically, the swath of
368 tornado reports in this case was limited on the poleward side by the rapidly increasing LCL
369 heights and decreasing CAPE and limited on the equatorward side by the rapidly decreasing
370 absolute vorticity along the cold front, in a prefrontal environment with adequate low-level wind
371 shear and storm-relative helicity all along the front. Although forecasting tornadoes along linear
372 convective systems remains a challenging forecast problem, this sweet spot may provide insight
373 into providing more specificity for nowcasting tornado development along future linear
374 convective systems in the U.K. or elsewhere.

375

376 **6. Model simulation: Misovortex structure and evolution**

377 The majority of tornado reports occurred within the model domain with 200-m horizontal
378 grid spacing as the modeled front passed through this domain between 1300 UTC and 1640 UTC
379 (Fig. 12). Analysis of vorticity, reflectivity, and surface winds from this domain exhibits more
380 detail along the front where the majority of tornado reports occurred. This region is also where
381 this apparent sweet spot favorable for tornadogenesis occurred.

382 At this higher resolution, more detail in the structure and evolution of the misovortices is
383 apparent. Specifically, regions of larger 500-m absolute vorticity ($0.02\text{--}0.03\text{ s}^{-1}$) developed into
384 maxima of $0.035\text{--}0.04\text{ s}^{-1}$ within the line, with 500-m updrafts of $5\text{--}10\text{ m s}^{-1}$ (e.g., Fig. 17).
385 Pairing of absolute vorticity maxima and minima was common both within the line and in a few
386 patches a little ahead of the line, where there was some higher reflectivity as well. Some
387 merging and splitting of downdrafts and maxima, which has been shown to increase vorticity
388 (Lee and Wilhelmson 1997a), was observed, as well. Background reflectivity of 35–45 dBZ
389 occurred within the rainband, with some patches of higher reflectivity of 50–55 dBZ. Similar to
390 the core-and-gap structures observed by Mulder (2015), the shapes of the misovortices at their
391 maximum intensity are quite similar to each other, specifically, an updraft (usually $5\text{--}10\text{ m s}^{-1}$)
392 located poleward of the misovortex and a downdraft ($3\text{--}6\text{ m s}^{-1}$, although some downdrafts were
393 as large as $6\text{--}9\text{ m s}^{-1}$) located equatorward of the misovortex.

394 Where the rainband looked like a hook or breaking wave at its edge, the misovortex was
395 typically located at the rear edge of the rainband in the area of lower reflectivity (10–15 dBZ),
396 and eventually developed a hook shape (Fig. 18). Many misovortices intensified at the center of
397 the rainband and weakened as they moved backwards relative to the rainband, leaving the
398 misovortices on the cold side. Some evolved from a line of vorticity that curled up and split into
399 two hooks often described as a broken-S (McAvoy et al. 2000; Clark 2011), signatures similar to
400 the line-echo wave pattern (Nolen 1959) and the frontal type of misovortices observed modeled
401 in squall lines (Jewett and Wilhelmson 2006). The hook-shaped echo is likely a response to the
402 circulation around the misovortex. The kinematics of misovortices appear similar to that of
403 supercells and may suggest that tornadoes along lines may form similar to that inside a supercell,

404 as suggested by Weisman and Trapp (2003). Further investigation is required to confirm
405 whether the dynamics are similar.

406 To estimate how important these hook-shaped cells were in the model, all the misovortices
407 with absolute vorticity greater than 0.02 s^{-1} were plotted every minute between 1350 and 1450
408 over the 200-m domain when the front was in the plotted area of Fig. 12 ($110 \times 70 \text{ km}$). Previous
409 simulations of vortices in different storm types have produced vortices about this magnitude. For
410 supercells, Adlerman et al. (1999) found vorticity up to 0.054 s^{-1} . For bow echoes, vorticity
411 magnitudes ranged from 0.009 to 0.02 s^{-1} (Weisman and Trapp 2003; Trapp and Weisman 2003;
412 Wheatley and Trapp 2008; Atkins and St. Laurent 2009). For narrow cold-frontal rainbands,
413 Smart and Browning (2009) found vorticity up to 0.04 s^{-1} . Although the modeled vorticity
414 magnitudes depend on the case, they also depend on model grid spacing with higher-resolution
415 models producing higher vorticity values. We determined that 0.02 s^{-1} was a good balance
416 between choosing a smaller value with vorticity maxima everywhere and choosing a higher
417 value with relatively few vorticity maxima. If the numbers of vortices and vortices with hooks
418 are calculated every ten minutes during that 60-minute period (seven times), then an average of
419 39 (with a standard deviation of 3) misovortices existed, of which 20.4% (with a standard
420 deviation of 2.6%) displayed hooks at any one time. Thus, this evolution is relatively common
421 with the model simulation.

422

423 **7. Reassessment of number of reports**

424 We can use the simulation, in conjunction with a re-examination of the reports, to re-
425 examine this event. First, according to the TORRO database, 58 of these reports (56% of the 104
426 reports) were later verified by TORRO experts, and classified as definite by them; the other 46

427 reports were deemed to show reasonable evidence of a tornado having occurred, but not enough
428 to be certain—these were classified as probable. So, the minimum number of credible tornadoes
429 was deemed to be 58.

430 Second, the remaining 46 probable tornado reports were examined for likely duplicate
431 reports. The following approach was followed. Each of the 46 probable reports was checked to
432 see if it might have duplicated another report. Duplicate reports were defined in this article as
433 those reports occurring close in space and time, generally 5 km or closer and reported at the same
434 time. Because the reports in the TORRO database are recorded by the hour, in practice this
435 meant tornadoes reported during the same hour. If the duplicate probable report overlapped with
436 a definite report, then the definite report was retained and the probable report was discarded. If
437 a definite tornado report with unknown intensity was combined with a probable tornado report
438 with known intensity, then the intensity was assigned to the single definite report. If the
439 duplicate probable report overlapped with another probable report, then the more trustworthy
440 probable report was retained and the other report was discarded. Those reports that had been
441 checked by TORRO experts or were possessing tornado tracks, direction of travel or high T-
442 scale value were deemed to be the most trustworthy and retained. This check reduced the
443 number of probable reports by 14 to 32. These two checks reduced the number of tornadoes on
444 23 November 1981 to as few as 58 and as many as 90 tornadoes (Fig. 19).

445 Does the simulation provide support for this many tornadoes? The innermost model domain
446 over a section of southeast England contained a subset of 52 of the 104 reports and included part
447 of the area targeted by Anglia Television with their 30 reports, which is why this area had a
448 relatively high percentage of probable reports (e.g., Fig. 1). The re-examination above reduced
449 these 52 reports to 42 tornadoes (22 definite and 20 probable tornadoes).

450 To produce tracks of these misovortices that might be parent circulations for tornadoes,
451 absolute vorticity greater than 0.02 s^{-1} was plotted every minute over the 200-m domain (Fig.
452 20a). Taking 30 min (± 2 min because the data interval is every minute) as an approximate
453 minimum lifetime for a parent misovortex to produce a tornado (e.g., Wakimoto and Wilson
454 1989; Brady and Szoke 1989), the number of misovortices produced by the model was counted.
455 This plot was repeated for absolute vorticity maxima greater than 0.025 s^{-1} , updrafts greater than
456 5, 6, and 7 m s^{-1} , and downdrafts greater than 2, 3, and 4 m s^{-1} (Fig. 20). The results of counting
457 these tracks are summarized in Table 1, which include the average and median duration of tracks
458 lasting 30 min or more (termed *long-lived*), and the longest duration and track lengths. These
459 results show a substantial number of long-lived tracks of various intensities (e.g., 9 misovortices
460 of 0.025 s^{-1} or more, 23 updrafts of 5 m s^{-1} or more, 10 downdrafts of 2 m s^{-1} or more). Most of
461 the model tracks were from the northwest (note the line of constant longitude in the panels in
462 Fig. 20), consistent with the TORRO reports of tracks being mostly from the northwest. A few
463 tracks from the west or southwest, however, were also present (e.g., Figs. 20a,c), which was also
464 consistent with a few tornado reports.

465 Although some of the tracks of misovortices with vorticity greater than or equal to 0.02 s^{-1}
466 on the 200-m grid are within 5 km of each other, tornado reports less than 5 km apart are more
467 likely to represent the same tornado than ones say 20 km apart. We can never claim that our
468 approach is perfect, but merely suggests a plausible way to filter possibly duplicate reports.
469 Also, there was some ambiguity in how the locations of the reports were recorded (which may
470 have been as specific as the name of a town, rather than a quantitative latitude–longitude
471 coordinate). Such ambiguities would complicate the assessment of the duplicate reports.
472 Finally, the tornado reports that were discounted were listed as only probable by TORRO, so

473 there is no risk of eliminating definite tornadoes. Thus, we are confident in the model's ability to
474 produce a large number of misovortices that are consistent with the large number of tornado
475 reports widespread over a large region of England and Wales.

476 If the tornadoes on this day developed from parent misovortices that were formed by the
477 tilting-shear mechanism (e.g., Trapp and Weismann, 2003), we would expect horizontal vorticity
478 to develop first, increase, be tilted vertically by an updraft–downdraft dipole, and then weaken.
479 Thus, we would expect the parent misocyclone to have a shorter lifetime than the updraft. From
480 Fig. 20 and Table 1, examples of tracks of updrafts ($5\text{--}10\text{ m s}^{-1}$) and tracks of vorticity greater
481 than 0.02 s^{-1} had similar lengths. The vorticity increased to above 0.025 s^{-1} along the tracks and
482 then toward the end of the tracks. Downdrafts of $3\text{--}6\text{ m s}^{-1}$ also appeared alongside these tracks
483 for shorter lengths than the updrafts and of only slightly shorter lengths than the higher vorticity
484 tracks. Counting the number of absolute vorticity maxima of 0.02 s^{-1} or more that last for 30 min
485 or longer yields 41 misovortices, with some of the longer-lasting updrafts forming multiple
486 misovortices. Of these 41 misovortices, 30 have updrafts of 5 m s^{-1} or more and downdrafts of 3
487 m s^{-1} or more each lasting longer than 4 min, meaning that there are roughly 30 possible parent
488 circulations in the 200-m domain alone (Fig. 21). Of these 30 tracks, the average lifetime of the
489 tracks was 47.6 min (median of 39 min), and the longest track was 175 km and lasted for 109
490 min. When linked with favorable environmental conditions for tornadogenesis in the model and
491 the results of Atkins et al. (2004) who found that tornadoes were more likely to form from parent
492 misovortices along the convective line that had greater rotation rates, the potential existed for the
493 model misovortices to have been tornadic. Thus, these roughly 30 intense misovortices within
494 the innermost domain are sufficient to explain the 22–44 tornado reports within this domain.

495 Figure 22 combines the half-hourly absolute vorticity isochrones with the regions with
496 favorable CAPE and vorticity values, and the observed 90 tornado reports. The majority of the
497 tornado reports (89 out of 90) were within the favorable locations (high vorticity along the cold
498 front and nonzero CAPE). Also, there was agreement between the modeled misocyclone tracks
499 and the locations of the tornado reports, providing additional veracity of the simulation. The
500 possibility also existed that these misovortices could have produced multiple tornadoes each.
501 Therefore, these statistics give an indication of the potential of high-resolution modeling to
502 resolve features potentially responsible for the tornadoes, as convection-permitting simulations
503 did 15 years ago for the 3 May 1999 Oklahoma–Kansas supercellular tornado outbreak (e.g.,
504 Roebber et al. 2002), and provides justification for a potentially large number of possible parent
505 circulations for tornadogenesis in this event.

506

507 **8. Conclusions**

508 The U.K. tornado outbreak of 23 November 1981 is analyzed from a convection-permitting
509 model simulation and a re-examination of the 104 tornado reports collected by TORRO. This
510 case is called “Britain’s greatest tornado outbreak” (Rowe and Meaden 1985) because its 104
511 reports were so much greater than the next highest outbreak of 29. A synoptic situation with a
512 strong cold front, weak CAPE (less than 125 J kg^{-1}), prefrontal winds nearly parallel to the front,
513 and postfrontal winds nearly perpendicular to the front is consistent with weather conditions
514 associated with other tornado outbreaks in the U.K. (Clark 2009; Clark and Parker 2014).

515 The model simulation produced a narrow cold-frontal rainband along a line of absolute
516 vorticity exceeding 0.02 s^{-1} on the 200-m grid with embedded maxima of $0.035\text{--}0.04 \text{ s}^{-1}$, similar
517 to those in previous simulations of misovortices along cold fronts in the U.K. (Smart and

518 Browning 2009). Misovortices along the front formed a variety of different structures and
519 evolutions and may have been parent circulations for the tornadoes. A line of reflectivity along
520 the cold front was characterized by precipitation cores and gaps. Updrafts of 5–10 m s⁻¹ occurred
521 poleward of these maxima of absolute vorticity, and weaker downdrafts of 3–6 m s⁻¹ occurred
522 equatorward, suggesting the potential for tilting to be involved in tornadogenesis.

523 The line of absolute vorticity weakened rapidly to the south in conjunction with a
524 weakened pressure trough. Nearly all of tornadoes reported occurred within a sweet spot where
525 the absolute vorticity was strong enough (more than 0.002 s⁻¹ on the 1-km grid) and the CAPE
526 was positive in an environment that was otherwise favorable for tornadoes (0–1-km storm-
527 relative helicity and 0–1-km shear). This approach suggests a means by which regions favorable
528 for tornadoes along squall lines could be forecast in the U.K. and elsewhere. The narrow (tens of
529 km) region of positive CAPE in advance of the front also raises concerns about large distances
530 used in determining proximity soundings in previous studies (100–200 km).

531 Within the model domain with 200-m horizontal grid spacing, 30 possible parent
532 misovortices were present with the following characteristics: absolute vorticity greater than 0.02
533 s⁻¹, updrafts between 5 and 10 m s⁻¹ for longer than 30 min, and downdrafts between 3 and 6 m
534 s⁻¹ were present for at least 4 min. This number of parent misovortices was comparable to the
535 figure of 22–44 tornado reports in this area. We conclude that the number of reports in this area
536 was potentially credible.

537 Reassessing the quality, timing and location of the reports allows us to place revised
538 boundaries on the lower and upper limit of the number of tornadoes that day. A final figure was
539 produced of 90 tornadoes: 58 definite and 32 probable, a slight reduction from the 104 total
540 reports. This revision does not eliminate the problem of the event distorting the historical record

541 (Mulder and Schultz 2015; Antonescu et al., 2016). Even if the lower limit were closer to 58
542 reports, this event would still be the largest documented tornado outbreak in the U.K.

543

544 *Acknowledgements:* We thank TORRO, in particular Terence Meaden and Paul Brown, for
545 providing the tornado data for 23 November 1981, and Jeff Trapp, David Smart, and an
546 anonymous reviewer for their comments that have improved this article. We thank ARCHER,
547 the U.K. National Supercomputing Service, for hosting the simulations. The historical weather
548 maps were provided by Mark Beswick of the National Meteorological Archive and Duncan Ball
549 of the Met Office Library, and we thank Stephen Burt for telling us about the existence of these
550 map archives. The satellite imagery was provided by Andrew Brooks and Neil Lonie of the
551 Dundee Satellite Receiving Station. Jonathan Fairman provided the CAPE value from the
552 NCEP–NCAR Reanalysis. Funding for Apsley was provided by the U.K. Natural Environment
553 Research Council through the Manchester–Liverpool Doctoral Training Programme Grant
554 NE/L002469/1. Funding for Mulder was provided by a scholarship from the Faculty of
555 Engineering and Physical Sciences, University of Manchester. Partial funding for Schultz was
556 provided by the Natural Environment Research Council to the University of Manchester through
557 Grants NE/H008225/1, NE/I005234/1, and NE/N003918/1 and by the Risk Prediction Initiative
558 of the Bermuda Institute of Ocean Sciences through Grant RPI2.0-2016-SCHULTZ.

559

560

REFERENCES

561 Adlerman, E. J., K. K. Droegemeier, and R. Davies-Jones, 1999: A numerical simulation of
562 cyclic mesocyclogenesis. *J. Atmos. Sci.*, **56**, 2045–2069.

563 Antonescu, B., D. M. Schultz, F. Lomas, and T. Kühne, 2016: Tornadoes in Europe: Synthesis of
564 the observational datasets. *Mon. Wea. Rev.*, doi: 10.1175/MWR-D-15-0298.1.

565 Atkins, N. T., and M. St. Laurent, 2009: Bow echo mesovortices. Part I: Processes that influence
566 their damaging potential. *Mon. Wea. Rev.*, **137**, 1497–1513.

567 Atkins, N. T., J. M. Arnott, R. W. Przybylinski, R. A. Wolf, and B. D. Ketcham, 2004: Vortex
568 structure and evolution within bow echoes. Part I: Single-Doppler and damage analysis of the
569 29 June 1998 derecho. *Mon. Wea. Rev.*, **132**, 2224–2242, doi: [10.1175/1520-
570 0493\(2004\)132<2224:VSAEWB>2.0.CO;2](https://doi.org/10.1175/1520-0493(2004)132<2224:VSAEWB>2.0.CO;2)

571 Bolton, N., D. M. Elsom, and G. T. Meaden, 2003: Forecasting tornadoes in the United
572 Kingdom. *Atmos. Res.*, **67–68**, 53–72, doi:10.1016/S0169-8095(03)00083-8.

573 Brady, R. H., and E. J. Szoke, 1989: A case study of non-mesocyclone tornado development in
574 northeast Colorado: Similarities to waterspout formation. *Mon. Wea. Rev.*, **117**, 843–856,
575 doi: 10.1175/1520-0493(1989)117<0843:ACSONT>2.0.CO;2.

576 Brooks, H. E., 2009: Proximity soundings for severe convection for Europe and the United States
577 from reanalysis data. *Atmos. Res.*, **93**, 546–553, doi:10.1016/j.atmosres.2008.10.005.

578 Brooks, H. E., and C. A. Doswell, 2001: Some aspects of the international climatology of
579 tornadoes by damage classification. *Atmos. Res.*, **56**, 191–201, doi: 10.1016/S0169-
580 8095(00)00098-3.

581 Brown, M. J., J. D. Locatelli, M. T. Stoelinga, and P. V. Hobbs, 1999: Numerical modeling of
582 precipitation cores on cold fronts. *J. Atmos. Sci.*, **56**, 1175–1196.

583 Browning, K. A., 1990: Organization of clouds and precipitation in extratropical cyclones.
584 *Extratropical Cyclones, The Erik Palmén Memorial Volume*, C. W. Newton and E. O.
585 Holopainen, Eds., Amer. Meteor. Soc., 129–153.

586 Browning, K. A., and T. W. Harrold, 1970: Air motion and precipitation growth at a cold front.
587 *Quart. J. Roy. Meteor. Soc.*, **96**, 369–389.

588 Browning, K. A., and C. W. Pardoe, 1973: Structure of low-level jet streams ahead of
589 mid-latitude cold fronts. *Quart. J. Roy. Meteor. Soc.*, **99**, 619–638.

590 Browning, K. A., and R. Reynolds, 1994: Diagnostic study of a narrow cold frontal rainband
591 and severe winds associated with a stratospheric intrusion. *Quart. J. Roy. Meteor. Soc.*, **120**,
592 235–257.

593 Browning, K. A., and N. M. Roberts, 1996: Variation of frontal and precipitation structure along
594 a cold front. *Quart. J. Roy. Meteor. Soc.*, **122**, 1845–1872.

595 Browning, K. A., N. M. Roberts, and A. J. Illingworth, 1997: Mesoscale analysis of the
596 activation of a cold front during cyclogenesis. *Quart. J. Roy. Meteor. Soc.*, **123**, 2349–2375.

597 Carbone, R. E., 1982: A severe frontal rainband. Part I. Stormwide hydrodynamic structure. *J.*
598 *Atmos. Sci.*, **39**, 258–279.

599 Carbone, R. E., 1983: A severe frontal rainband. Part II. Tornado parent vortex circulation. *J.*
600 *Atmos. Sci.*, **40**, 2639–2654.

601 Clark, M. R., 2009: The southern England tornadoes of 30 December 2006: Case study of a
602 tornadic storm in a low CAPE, high shear environment. *Atmos. Res.*, **93**, 50–65,
603 doi:10.1016/j.atmosres.2008.10.008.

604 Clark, M. R., 2011: Doppler radar observations of mesovortices within a cool-season tornadic
605 squall line over the UK. *Atmos. Res.*, **100**, 749–764, doi:10.1016/j.atmosres.2010.09.007.

606 Clark, M. R., 2013: A provisional climatology of cool-season convective lines in the UK. *Atmos.*
607 *Res.*, **123**, 180–196, doi:10.1016/j.atmosres.2012.09.018.

608 Clark, M. R., and D. J. Parker, 2014: On the mesoscale structure of surface wind and pressure
609 fields near tornadic and nontornadic cold fronts. *Mon. Wea. Rev.*, **142**, 3560– 3585, doi:
610 10.1175/MWR-D-13-00395.1.

611 Craven, J. P., and H. E Brooks, 2004: Baseline climatology of sounding derived parameters
612 associated with deep moist convection. *Natl. Wea. Dig.*, **28**, 13–24.

613 Doe, R. K., Ed., 2016: *Extreme Weather: Forty Years of the Tornado and Storm Research*
614 *Organization (TORRO)*. Wiley Blackwell, 327 pp.

615 Elsom, D. M., G. T. Meaden, D. J. Reynolds, M. W. Rowe, and J. D. C. Webb, 2001: Advances
616 in tornado and storm research in the United Kingdom and Europe: The role of the Tornado
617 and Storm Research Organisation. *Atmos. Res.*, **56**, 19–29, doi:10.1016/S0169-
618 8095(00)00084-3.

619 Fujita, T., 1981: Tornadoes and downbursts in the context of generalized planetary scales. *J.*
620 *Atmos. Sci.*, **38**, 1511–1534.

621 Groenemeijer, P., U. Corsmeier, and Ch. Kottmeier, 2011: The development of tornadic storms
622 on the cold side of a front favoured by local enhancement of moisture and CAPE. *Atmos.*
623 *Res.*, **100**, 765–781, doi:10.1016/j.atmosres.2010.10.028.

624 Hagan, M., 1992: On the appearance of a cold front with a narrow rainband in the vicinity of the
625 Alps. *Meteor. Atmos. Phys.*, **48**, 231–248.

626 Hobbs, P. V., and K. R. Biswas, 1979: The cellular nature of narrow cold-frontal rainbands.
627 *Quart. J. Roy. Meteor. Soc.*, **105**, 723–727.

628 Hobbs, P. V., and P. O. G. Persson, 1982: The mesoscale and microscale structure and
629 organization of clouds and precipitation in midlatitude cyclones. Part V: The substructure of
630 narrow cold-frontal rainbands. *J. Atmos. Sci.*, **39**, 280–295.

631 Holden, J., and A. Wright, 2004: Tornado climatology and the development of simple prediction
632 tools. *Quart. J. Roy. Meteor. Soc.*, **130**, 1009–1021, doi: 10.1256/qj.03.45.

633 Houze, R. A., Jr., 2014: *Cloud Dynamics*, 2nd ed. Academic Press, 496 pp.

634 James, P. K., and K. A. Browning, 1979: Mesoscale structure of line convection at surface cold
635 fronts. *Quart. J. Roy. Meteor. Soc.*, **105**, 371–382.

636 Janjić, Z. I., 1994: The step-mountain eta coordinate model: Further developments of the
637 convection, viscous sublayer and turbulence closure schemes. *Mon. Wea. Rev.*, **122**, 927–
638 945, doi: 10.1175/1520-0493(1994)122<0927:TSMECM>2.0.CO;2.

639 Janjić, Z. I., 2002: Nonsingular implementation of the Mellor–Yamada level 2.5 scheme in the
640 NCEP Meso model. NCEP Office Note, No. 437, 61 pp.

641 Jewett, B. F., and R. B. Wilhelmson, 2006: The role of forcing in cell morphology and evolution
642 within midlatitude squall lines. *Mon. Wea. Rev.*, **134**, 3714–3734.

643 Johns, R. H., and C. A. Doswell III, 1992: Severe local storms forecasting. *Wea. Forecasting*, **7**,
644 588–612, doi: 10.1175/1520-0434(1992)007<0588:SLSF>2.0.CO;2.

645 Jorgensen, D. P., Z. Pu, P. O. G. Persson, and W. Tao, 2003: Variations associated with cores
646 and gaps of a Pacific narrow cold frontal rainband. *Mon. Wea. Rev.*, **131**, 2705–2729, doi:
647 10.1175/1520-0493(2003)131<2705:VAWCAG>2.0.CO;2.

648 Kain, J. S., 2004: The Kain–Fritsch convective parameterization: An update. *J. Appl. Meteor.*,
649 **43**, 170–181, doi: 10.1175/1520-0450(2004)043<0170:TKCPAU>2.0.CO;2.

650 Kain, J. S., and J. M. Fritsch, 1990: A one-dimensional entraining/detraining plume model and
651 its application in convective parameterization. *J. Atmos. Sci.*, **47**, 2784–2802, doi:
652 10.1175/1520-0469(1990)047<2784:AODEPM>2.0.CO;2.

653 Kalnay, E., and Coauthors, 1996: The NCEP/NCAR 40-Year Reanalysis Project. *Bull. Amer.*
654 *Meteor. Soc.*, **77**, 437–471.

655 Kawashima, M., 2011: Numerical study of horizontal shear instability waves along narrow cold
656 frontal rainbands. *J. Atmos. Sci.*, **68**, 878–903.

657 Kemp, A. K., and S. J. Morris, 1982: Line squall and minor tornadoes at Holyhead, 23
658 November 1981. *Meteor. Mag.*, **111**, 253–261.

659 Kirk, P. J., 2014: An updated tornado climatology for the UK: 1981–2010. *Weather*, **69**, 171–
660 175.

661 Kobayashi, F., Y. Sugawara, M. Imai, M. Matsui, A. Yoshida, and Y. Tamura, 2007: Tornado
662 generation in a narrow cold frontal rainband—Fujisawa tornado on April 20, 2006—. *SOLA*,
663 **3**, 21–24.

664 Lee, B. D., and R. B. Wilhelmson, 1997a: The numerical simulation of non-supercell
665 tornadogenesis. Part I: Initiation and evolution of pretornadic misocyclone and circulations
666 along a dry outflow boundary. *J. Atmos. Sci.*, **54**, 32–60.

667 Lee, B. D., and R. B. Wilhelmson, 1997b: The numerical simulation of nonsupercell
668 tornadogenesis. Part II: Evolution of a family of tornadoes along a weak outflow boundary. *J.*
669 *Atmos. Sci.*, **54**, 2387–2415.

670 Lee, B. D., and R. B. Wilhelmson, 2000: The numerical simulation of nonsupercell
671 tornadogenesis. Part III: Parameter tests investigating the role of CAPE, vortex sheet
672 strength, and boundary layer vertical shear. *J. Atmos. Sci.*, **57**, 2246–2261.

673 Locatelli, J. D., J. E. Martin, and P. V. Hobbs, 1995: Development and propagation of
674 precipitation cores on cold fronts. *Atmos. Res.*, **38**, 177–206.

675 Markowski, P. M., J. M. Straka, and E. N. Rasmussen, 2002: Direct surface thermodynamic
676 observations within the rear-flank downdrafts of nontornadic and tornadic supercells. *Mon.*
677 *Wea. Rev.*, **130**, 1692–1721, doi: 10.1175/1520-0493(2002)130<1692:DSTOWT>2.0.CO;2.

678 McAvoy, B. P., W. A. Jones, and P. D. Moore, 2000: Investigation of an unusual storm structure
679 associated with weak to occasionally strong tornadoes over the eastern United States.
680 Preprints, *20th Severe Local Storms Conference*, Orlando, FL, Amer. Meteor. Soc., 182–185.

681 Meaden, G. T., 1983: The TORRO tornado intensity scale. *J. Meteor. (UK)*, **8**, 151–153.

682 Meaden, G. T., S. Kochev, L. Kolendowicz, A. Kosa-Kiss, I. Marcinoniene, M. Sioutas, H.
683 Tooming, and J., Tyrrell, 2007: Comparing the theoretical versions of the Beaufort scale, the
684 T-Scale and the Fujita scale. *Atmos. Res.*, **83**, 446–449, doi:10.1016/j.atmosres.2005.11.014.

685 Mellor, G. L., and T. Yamada, 1982: Development of a turbulence closure model for geophysical
686 fluid problems. *Rev. Geophys. Space Phys.*, **20**, 851–875.

687 Morrison, H., G. Thompson, and V. Tatarskii, 2009: Impact of cloud microphysics on the
688 development of trailing stratiform precipitation in a simulated squall line: Comparison of
689 one- and two-moment schemes. *Mon. Wea. Rev.*, **137**, 991–1007.

690 Mulder, K. J., 2015: Tornadoes in the British Isles: Climatology, formation environments, and
691 storm dynamics. Ph.D. dissertation, University of Manchester, 96 pp.

692 Mulder, K. J., and D. M. Schultz, 2015: Climatology, storm morphologies, and environments of
693 tornadoes in the British Isles: 1980–2012. *Mon. Wea. Rev.*, **143**, 2224–2240.

694 Nolen, R. H., 1959: A radar pattern associated with tornadoes. *Bull. Amer. Meteor. Soc.*, **40**,
695 277–279.

696 Potvin, C. K., K. L. Elmore, and S. J. Weiss, 2010: Assessing the impacts of proximity sounding
697 criteria on the climatology of significant tornado environments. *Wea. Forecasting*, **25**, 921–
698 930.

699 Púčik, T., P. Groenemeijer, D. Rýva, and M. Kolář, 2015: Proximity soundings of severe and
700 nonsevere thunderstorms in Central Europe. *Mon. Wea. Rev.*, **143**, 4805–4821.

701 Rasmussen, E. N., and D. O. Blanchard, 1998: A baseline climatology of sounding-derived
702 supercell and tornado forecast parameters. *Wea. Forecasting*, **13**, 1148–1164.

703 Roebber, P. J., D. M. Schultz, and R. Romero, 2002: Synoptic regulation of the 3 May 1999
704 tornado outbreak. *Wea. Forecasting*, **17**, 399–429.

705 Rowe, M. W., 1985: Britain’s greatest tornadoes and tornado outbreak. *J. Meteor. (UK)*, **10**,
706 212–220.

707 Rowe, M. W., 2016: Tornado extremes in the United Kingdom: The earliest, longest, widest,
708 severest, and deadliest. *Extreme Weather: Forty Years of the Tornado and Storm Research*
709 *Organization (TORRO)*. R. K. Doe, Ed., Wiley Blackwell, 77–90.

710 Rowe, M. W., and G. T. Meaden, 1985: Britain’s greatest tornado outbreak. *Weather*, **40**, 230–
711 235, doi: 10.1002/j.1477-8696.1985.tb06883.x.

712 Skamarock, W. C., J. B. Klemp, J. Dudhia, D. O. Gill, D. M. Barker, M. G. Duda, X.-Y. Huang,
713 W. Wang, and J. G. Powers, 2008: A description of the Advanced Research WRF Version 3.
714 NCAR technical note, NCAR/TN-475+STR, 113 pp.

715 Smart, D. J., and K. A. Browning, 2009: Morphology and evolution of cold-frontal
716 misocyclones. *Quart. J. Roy. Meteor. Soc.*, **135**, 381–393, doi: 10.1002/qj.399.

717 Smith, B. T., R. L. Thompson, J. S. Grams, C. Broyles, and H. E. Brooks, 2012: Convective
718 modes for significant severe thunderstorms in the contiguous United States. Part I: Storm
719 classification and climatology. *Wea. Forecasting*, **27**, 1114–1135, doi: [10.1175/WAF-D-11-](https://doi.org/10.1175/WAF-D-11-00115.1)
720 [00115.1](https://doi.org/10.1175/WAF-D-11-00115.1).

721 Speheger, D. A., C. A. Doswell III, and G. J. Stumpf, 2002: The tornadoes of 3 May 1999:
722 Event verification in central Oklahoma and related issues. *Wea. Forecasting*, **17**, 362–381.

723 Sugawara, Y., and F. Kobayashi, 2009: Vertical structure of misocyclones along a narrow cold
724 frontal rainband. *J. Meteor. Soc. Japan*, **87**, 497–503.

725 Thompson, G., P. R. Field, R. M. Rasmussen, and W. D. Hall, 2008: Explicit forecasts of winter
726 precipitation using an improved bulk microphysics scheme. Part II: Implementation of a new
727 snow parameterization. *Mon. Wea. Rev.*, **136**, 5095–5115, doi:10.1175/2008MWR2387.1.

728 Thompson, R. L., R. Edwards, J. A. Hart, K. L. Elmore, and P. Markowski, 2003: Close
729 proximity soundings within supercell environments obtained from the Rapid Update Cycle.
730 *Wea. Forecasting*, **18**, 1243–1261.

731 Thompson, R. L., B. T. Smith, J. S. Grams, A. R. Dean, and C. Broyles, 2012: Convective modes
732 for significant severe thunderstorms in the contiguous United States. Part II: Supercell and
733 QLCS tornado environments. *Wea. Forecasting*, **27**, 1136–1154.

734 Trapp, R. J., E. D. Mitchell, G. A. Tipton, D. W. Effertz, A. I. Watson, D. L. Andra Jr., and M.
735 A. Magsig, 1999: Descending and non-descending tornadic vortex signatures detected by
736 WSR-88Ds. *Wea. Forecasting*, **14**, 625–639.

737 Trapp, R. J., S. A. Tessendorf, E. S. Godfrey, and H. E. Brooks, 2005: Tornadoes from squall
738 lines and bow echoes. Part I: Climatological distribution. *Wea. Forecasting*, **20**, 23–34, doi:
739 10.1175/WAF-835.1.

740 Trapp, R. J., and M. L. Weisman, 2003: Low-level mesovortices within squall lines and bow
741 echoes. Part II: Their genesis and implications. *Mon. Wea. Rev.*, **131**, 2804–2823.

742 Trapp, R. J., D. M. Wheatley, N. T. Atkins, R. W. Przybylinski, and R. Wolf, 2006: Buyer
743 beware: Some words of caution on the use of severe wind reports in postevent assessment
744 and research. *Wea. Forecasting*, **21**, 408–415.

745 Turner, S., Elsom, D. M., and G. T. Meaden, 1986: An outbreak of 31 tornadoes associated with
746 a cold front in southern England on 20 October 1981. *J. Meteor. (UK)*, **11**, 37–50.

747 Viale, M., R. A. Houze Jr., and K. L. Rasmussen, 2013: Upstream orographic enhancement of a
748 narrow cold-frontal rainband approaching the Andes. *Mon. Wea. Rev.*, **141**, 1708–1730.

749 Wakimoto, R. M., and B. L. Bosart, 2000: Airborne radar observations of a cold front during
750 FASTEX. *Mon. Wea. Rev.*, **128**, 2447–2470.

751 Wakimoto, R. M., and J. W. Wilson, 1989: Non-supercell tornadoes. *Mon. Wea. Rev.*, **117**,
752 1113–1140.

753 Weisman, M. L., and R. J. Trapp, 2003: Low-level meso-vortices within squall lines and bow
754 echoes. Part I: Overview and dependence on environmental shear. *Mon. Wea. Rev.*, **131**,
755 2779–2803.

756 Wheatley, D. M., and R. J. Trapp, 2008: The effect of mesoscale heterogeneity on the genesis
757 and structure of mesovortices within quasi-linear convective systems. *Mon. Wea. Rev.*, **136**,
758 4220–4241.

759

760 **FIGURE CAPTIONS**

761 Figure 1. Locations of the 104 tornado reports from the TORRO database for 23 November
762 1981. Numbers represent their strength on the T scale; U represents unknown intensity, and
763 half-values represent intensities between two classes (e.g., 2.5 represents T2–T3). Reports
764 verified by TORRO (58) are classified as definite and plotted in black. Reports that have not
765 been verified (46) are classified as probable and are plotted in red. Locations discussed in the
766 text are labeled in blue. Locations of reports that appear to be located over water are a result of a
767 coarse representation of geography.

768 Figure 2. Distribution on the T scale of intensities of the 99 tornado reports on 23 November
769 1981 associated with an intensity rating from the TORRO database.

770 Figure 3. Excerpts from Met Office Daily Weather Summary surface weather charts at (a) 1200
771 UTC 22 November 1981 and (b) 1200 UTC 23 November 1981. Plotted are sea level pressure
772 contours every 4 hPa, surface fronts, surface temperatures (°C) and weather at selected cities,
773 and occasionally wind barbs (standard notation). Crown copyright.

774 Figure 4. Excerpt from Met Office Daily Weather Summary 500-hPa chart at 1200 UTC 23
775 November 1981. Plotted are 500-hPa geopotential height (solid lines every 6 dam) and 1000–
776 500-hPa thickness (dashed lines every 6 dam). Crown copyright.

777 Figure 5. Excerpts from the Met Office Central Forecasting Office hourly U.K. working charts at
778 (a) 1000 UTC, (b) 1200 UTC, and 1400 UTC 23 November 1981. Plotted are sea-level pressure
779 (solid lines every 2 hPa in (a) and (c) and 4 hPa in (b)), cold front (dashed line), and standard
780 station models. Crown copyright.

781 Figure 6. Hourly rainfall amounts (mm) from 213 rain gauges ending at 1200 UTC and 212 rain
782 gauges ending at 1400 UTC 23 Nov 1981.

783 Figure 7. Infrared satellite imagery (channel 5, 11.5–12.5 μm) at 1325 UTC 23 Nov 1981
784 (courtesy of Dundee Satellite Receiving Station).

785 Figure 8. Prefrontal sounding from Aughton, near Liverpool, at 0000 UTC 23 November 1981
786 (courtesy of the University of Wyoming, <http://weather.uwyo.edu/upperair/sounding.html>).

787 Figure 9. The two innermost domains used in this simulation.

788 Figure 10. Simulation of sea level pressure (hPa, blue lines), surface temperature ($^{\circ}\text{C}$, colored
789 according to scale), and surface winds (pennant, full barb, and half-barb denote 25, 5, 2.5 m s^{-1} ,
790 respectively; separation between displayed wind vectors is 30 km) on the domain with 1-km
791 horizontal grid spacing at (a) 1000 UTC and (b) 1400 UTC 23 November 1981.

792 Figure 11. Simulation of radar reflectivity factor (dBZ, colored according to scale) and surface
793 winds (pennant, full barb, and half-barb denote 25, 5, 2.5 m s^{-1} , respectively; separation between
794 displayed wind vectors is 30 km) on the domain with 1-km horizontal grid spacing at (a) 1000
795 UTC and (b) 1400 UTC 23 November 1981.

796 Figure 12. Simulation of absolute vorticity at 500 m ASL (s^{-1} , colored according to scale) every
797 30 min from 0930 UTC to 1730 UTC (labeled every hour) on the domain with 1-km horizontal
798 grid spacing. The red box indicates the location of the domain with 200-m horizontal grid
799 spacing.

800 Figure 13. Simulation of CAPE ($J kg^{-1}$, colored according to scale) and surface winds (pennant,
801 full barb, and half-barb denote 25, 5, 2.5 $m s^{-1}$, respectively; separation between displayed wind
802 vectors is 30 km) on the domain with 1-km horizontal grid spacing at (a) 1000 UTC and (b) 1400
803 UTC 23 November 1981.

804 Figure 14. Simulation of lifting condensation level (LCL) (m, colored according to scale) and
805 surface winds (pennant, full barb, and half-barb denote 25, 5, 2.5 $m s^{-1}$, respectively; separation
806 between displayed wind vectors is 30 km) on the domain with 1-km horizontal grid spacing at (a)
807 1000 UTC and (b) 1400 UTC 23 November 1981.

808 Figure 15. Simulation of 0–1-km vertical shear of the horizontal wind in magnitude ($m s^{-1}$,
809 colored according to scale) and direction (pennant, full barb, and half-barb denote 25, 5, 2.5 $m s^{-1}$,
810 respectively; separation between displayed wind vectors is 30 km) on the domain with 1-km
811 horizontal grid spacing at (a) 1000 UTC and (b) 1400 UTC 23 November 1981.

812 Figure 16. Simulation of 0–1-km storm-relative helicity ($m^2 s^{-2}$, colored according to scale) and
813 surface winds (pennant, full barb, and half-barb denote 25, 5, 2.5 $m s^{-1}$, respectively; separation
814 between displayed wind vectors is 30 km) on the domain with 1-km horizontal grid spacing at (a)
815 1000 UTC and (b) 1400 UTC 23 November 1981.

816 Figure 17. Simulation of radar reflectivity factor (black lines every 10 dBZ), absolute vorticity at
817 500 m ASL (positive values are contoured in dark blue solid lines every 0.005 s^{-1} , starting from
818 0.01 s^{-1} ; negative values are contoured in light blue solid lines every -0.005 s^{-1} every 0.005 s^{-1}),
819 500-m updrafts (red fill above 5 m s^{-1}), and 500-m downdrafts (green fill above 2 m s^{-1}) from the
820 200-m horizontal grid spacing domain, plotted every minute from 1431:50 to 1434:50 UTC 23
821 November 1981.

822 Figure 18. Characteristic structure and evolution of a simulated misovortex within the domain at
823 200-m horizontal grid spacing, plotted every 60 s around the time that it matures: radar
824 reflectivity factor (dBZ, colored according to scale in Fig. 16), absolute vorticity at 500 m ASL
825 (black contours every 0.005 s^{-1} , starting from 0.01 s^{-1}), 500-m updraft (red contours every 5 m s^{-1})
826 1), and 500-m downdraft (pink contours every 2 m s^{-1}). Each panel is about $4 \text{ km} \times 4 \text{ km}$, and
827 the vortex is about 500 m across.

828 Figure 19. Locations of the 90 revised tornado reports from the TORRO database for 23
829 November 1981. Numbers represent their strength on the T scale. Reports verified by TORRO
830 (58) are classified as definite and plotted in black. Reports that have not been verified (32) are
831 classified as probable and are plotted in red. Locations discussed in the text are labeled in blue.
832 The red box indicates the location of the domain with 200-m horizontal grid spacing. Locations
833 of reports that appear to be located over water are a result of a coarse representation of
834 geography.

835 Figure 20. Tracks of (a) 500-m absolute vorticity (0.02 and 0.025 s^{-1}), (b) 500-m updrafts (5 , 6 ,
836 and 7 m s^{-1}), and (c) 500-m downdrafts (2 , 3 , and 4 m s^{-1}) plotted every minute from 1300 to
837 1600 UTC in the domain with 200-m horizontal grid spacing.

838 Figure 21. Simulation of 0.02 s^{-1} and 0.025 s^{-1} absolute vorticity at 500 m ASL (black contours),
839 5 m s^{-1} updrafts at 500 m (red contours), and 3 m s^{-1} downdrafts at 500 m (green contours) from
840 1300 to 1600 UTC on the domain with 200-m horizontal grid spacing.

841 Figure 22. Simulation of absolute vorticity at 500 m ASL (s^{-1} , colored according to scale) every
842 30 min from 0930 UTC to 1730 UTC on the domain with 1-km horizontal grid spacing. Purple
843 lines separate approximate areas with simulated absolute vorticity less than 0.002 s^{-1} on the 1-km
844 domain during the time of frontal passage. Blue lines separate approximate areas with simulated
845 positive CAPE during the time of frontal passage. Locations of reports that appear to be located
846 over water are a result of a coarse representation of geography. Locations of the 90 tornado
847 reports from the TORRO database for 23 November 1981. Numbers represent their strength on
848 the T scale. Reports verified by TORRO (58) are classified as definite and plotted in black.
849 Reports that have not been verified (32) are classified as probable and are plotted in red.

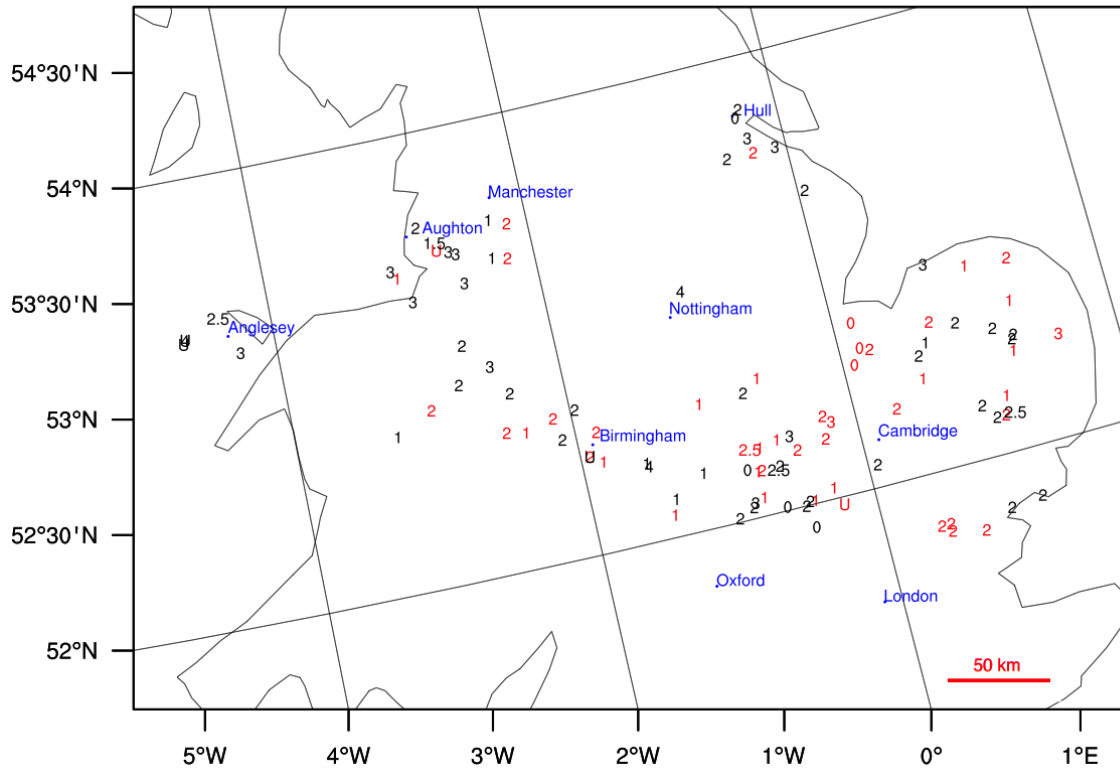
850

851 Table 1: Properties of tracks of 500-m absolute vorticity (0.02 and 0.025 s^{-1}), updrafts (5, 6, and
852 7 ms^{-1}), and downdrafts (2, 3, and 4 m s^{-1}) in the domain with 200-m horizontal grid spacing
853 between 1300 and 1600 UTC. “Long-lived” refers to features lasting 30 min or more (± 2 min
854 because the data interval is every minute). The longest duration track being listed as “101+”
855 means that a track started within the plotting domain but continued to the edge of the domain,
856 indicating that the track could have existed longer than 101 min. “N/A” represents no features
857 meeting the designated criteria.

	Number of long-lived maxima	Average duration of long-lived tracks (min)	Median duration of long-lived tracks (min)	Longest duration track (min)	Longest track length (to nearest 5 km)
Vorticity ($>0.025 \text{ s}^{-1}$) tracks	9	33.2	33	38	45
Vorticity ($>0.02 \text{ s}^{-1}$) tracks	41	40.3	37	64	75
Updrafts ($> 5 \text{ m/s}$) tracks	23	55.3	48	101+	175
Updrafts ($> 6 \text{ m/s}$) tracks	5	54.2	56	76	100
Updraft ($> 7 \text{ m/s}$) tracks	0	N/A	N/A	28	35
Downdrafts ($> 2 \text{ m/s}$) tracks	10	34.2	33.5	40	75
Downdrafts ($> 3 \text{ m/s}$) tracks	0	N/A	N/A	22	35
Downdrafts ($> 4 \text{ m/s}$) tracks	0	N/A	N/A	12	20

858

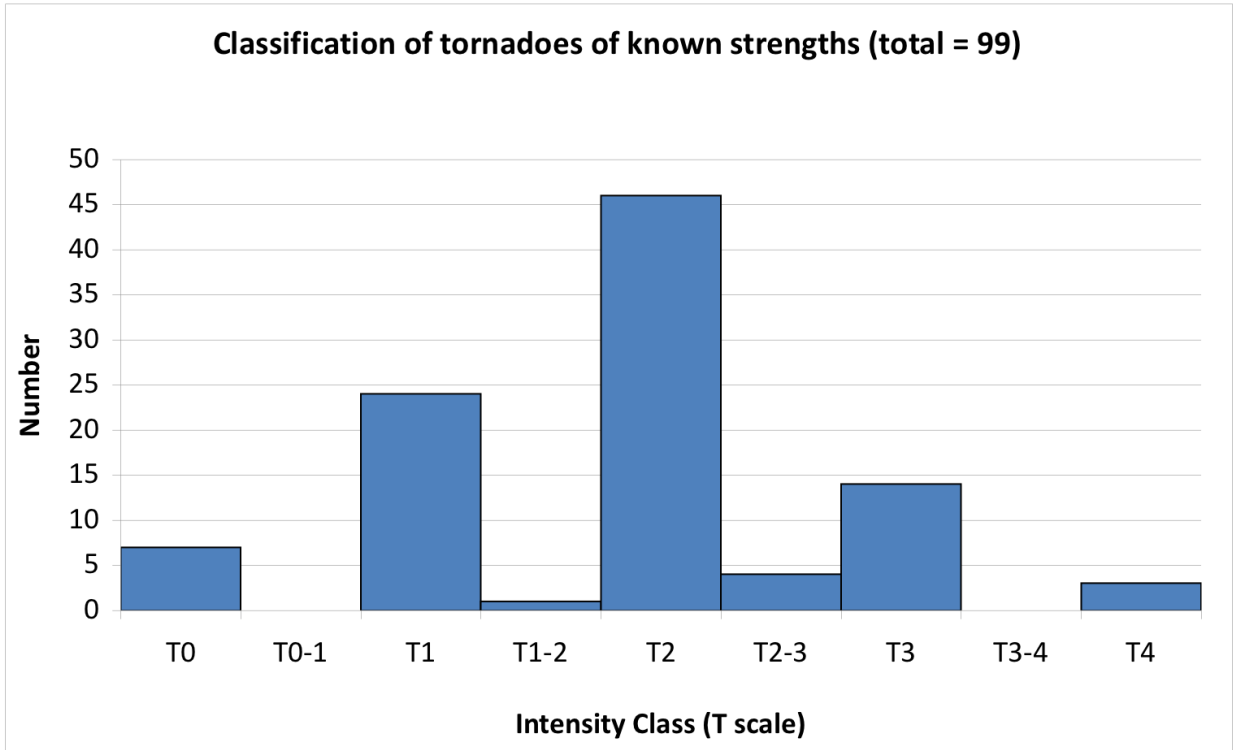
Locations of 104 Tornado Reports for 23 Nov 1981



860

861 Figure 1. Locations of the 104 tornado reports from the TORRO database for 23 November
 862 1981. Numbers represent their strength on the T scale; U represents unknown intensity, and
 863 half-values represent intensities between two classes (e.g., 2.5 represents T2–T3). Reports
 864 verified by TORRO (58) are classified as definite and plotted in black. Reports that have not
 865 been verified (46) are classified as probable and are plotted in red. Locations discussed in the
 866 text are labeled in blue. Locations of reports that appear to be located over water are a result of a
 867 coarse representation of geography.

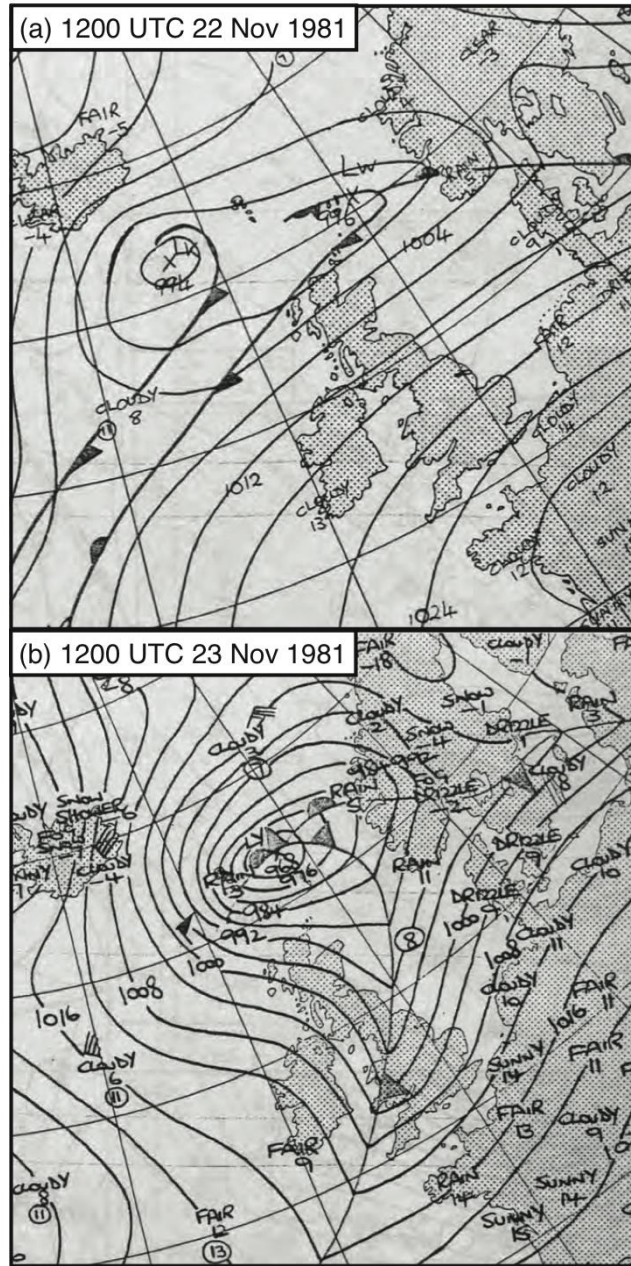
868



869

870 Figure 2. Distribution on the T scale of intensities of the 99 tornado reports on 23 November
 871 1981 associated with an intensity rating from the TORRO database.

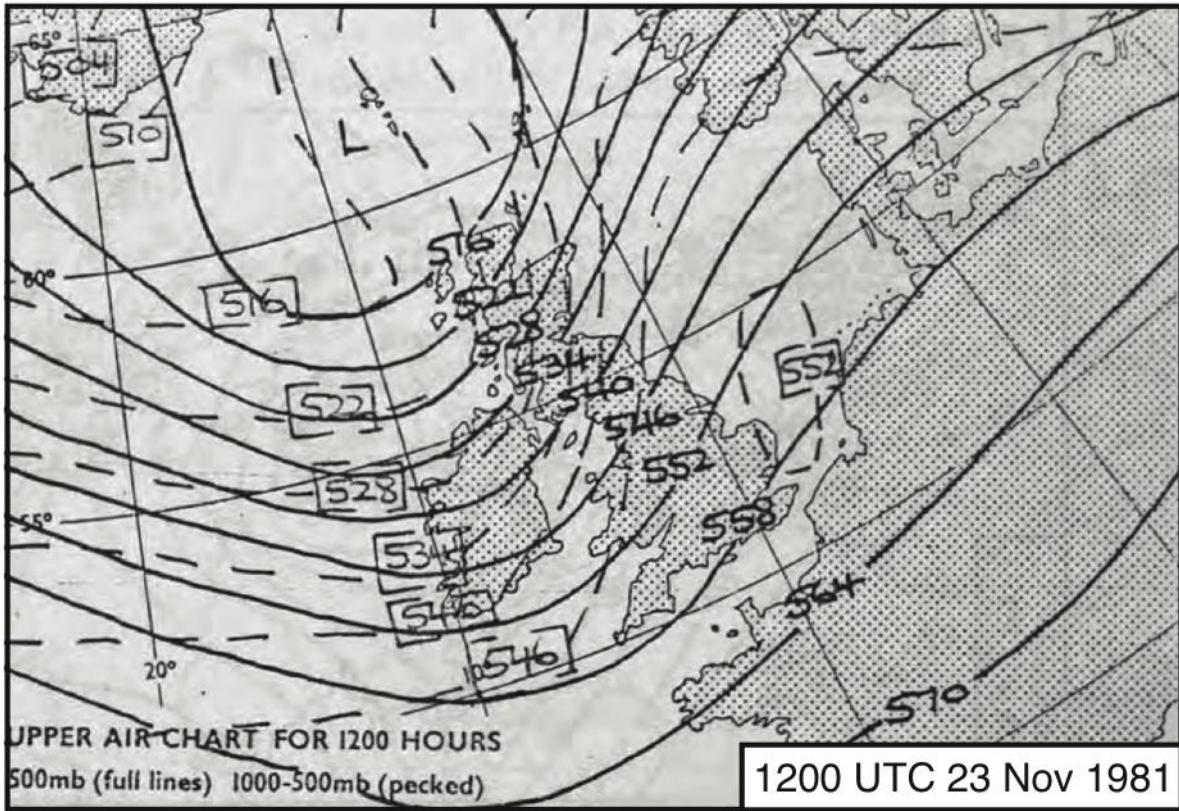
872



873

874 Figure 3. Excerpts from Met Office Daily Weather Summary surface weather charts at (a) 1200
 875 UTC 22 November 1981 and (b) 1200 UTC 23 November 1981. Plotted are sea level pressure
 876 contours every 4 hPa, surface fronts, surface temperatures ($^{\circ}\text{C}$) and weather at selected cities,
 877 and occasionally wind barbs (standard notation). Crown copyright.

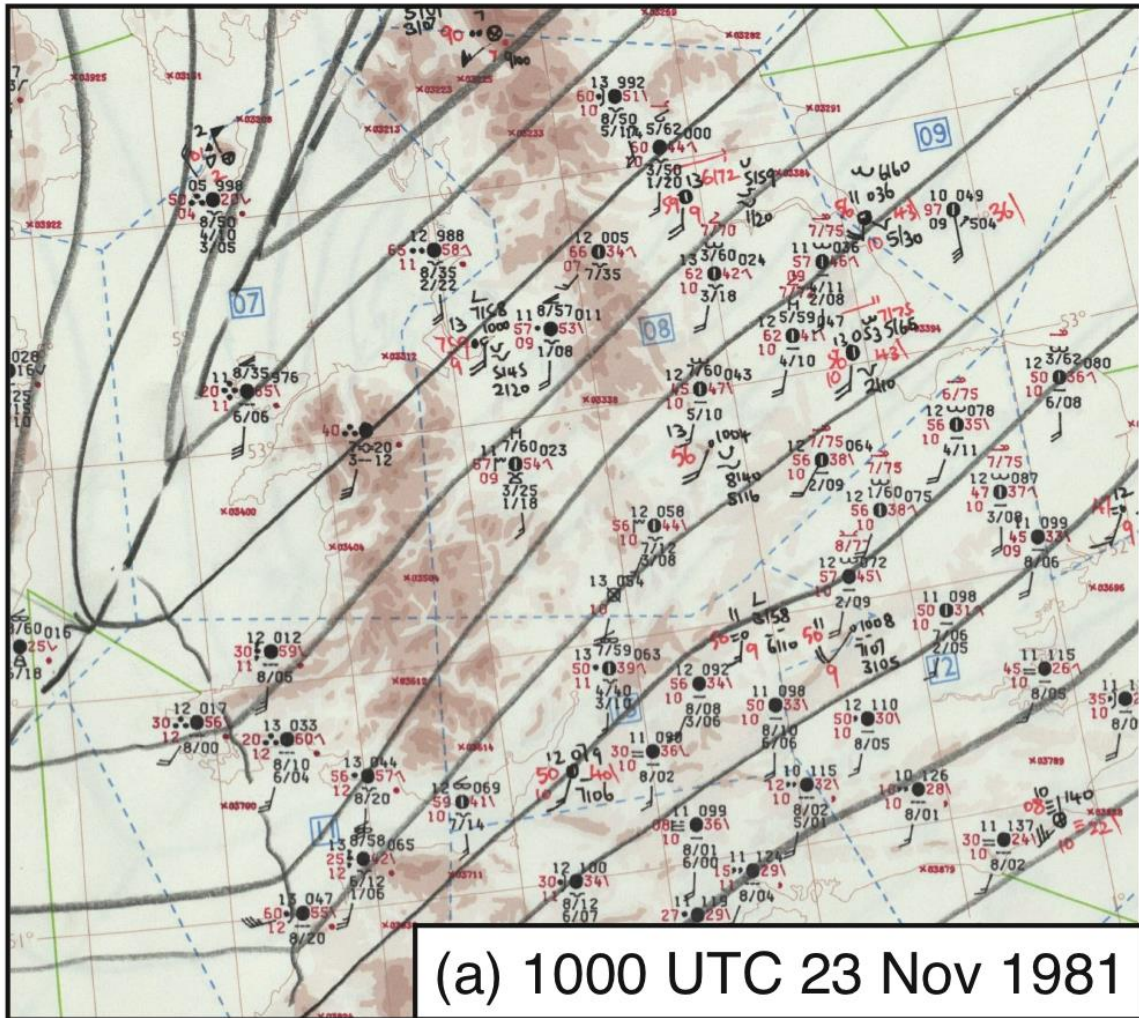
878



879

880 Figure 4. Excerpt from Met Office Daily Weather Summary 500-hPa chart at 1200 UTC 23
 881 November 1981. Plotted are 500-hPa geopotential height (solid lines every 6 dam) and 1000–
 882 500-hPa thickness (dashed lines every 6 dam). Crown copyright.

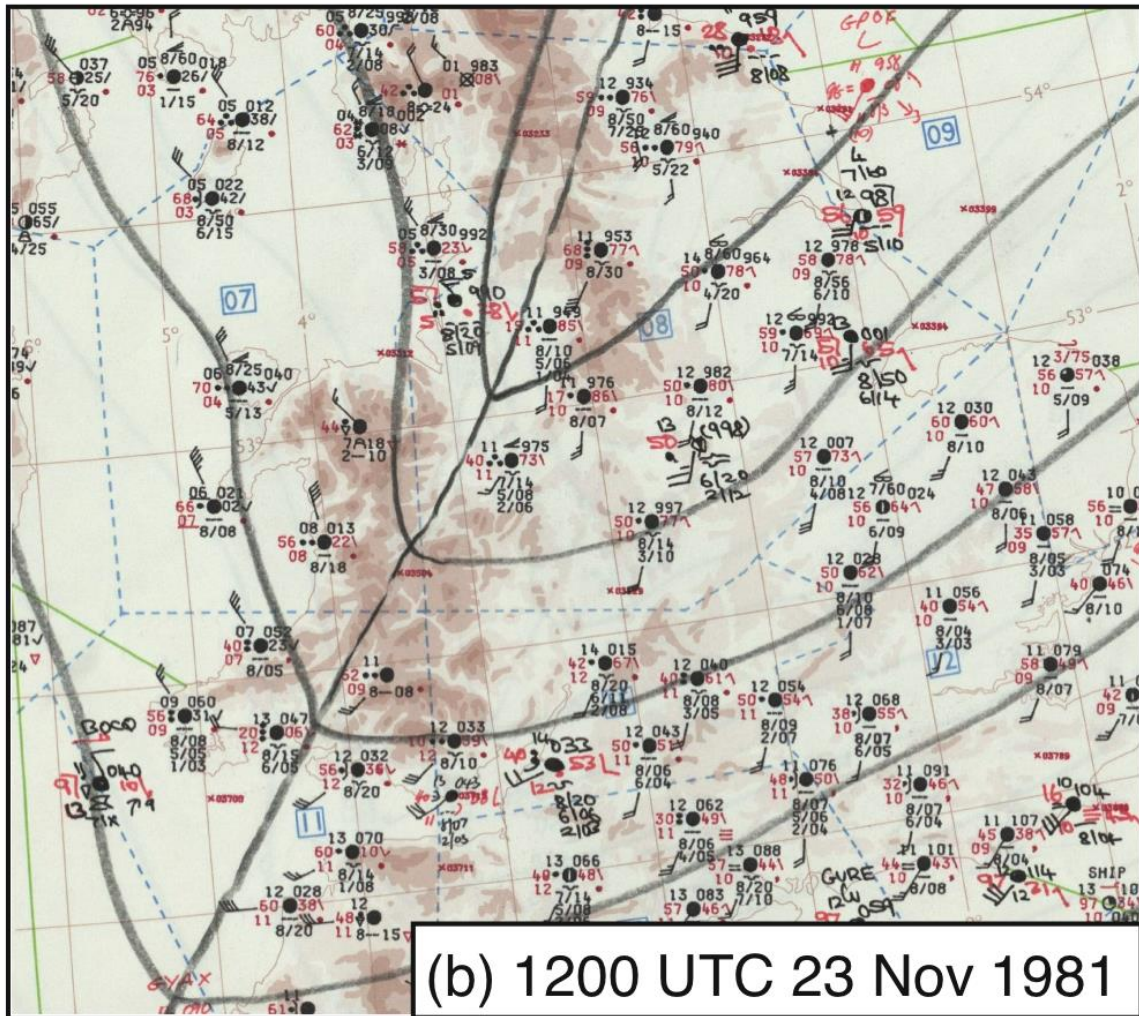
883



(a) 1000 UTC 23 Nov 1981

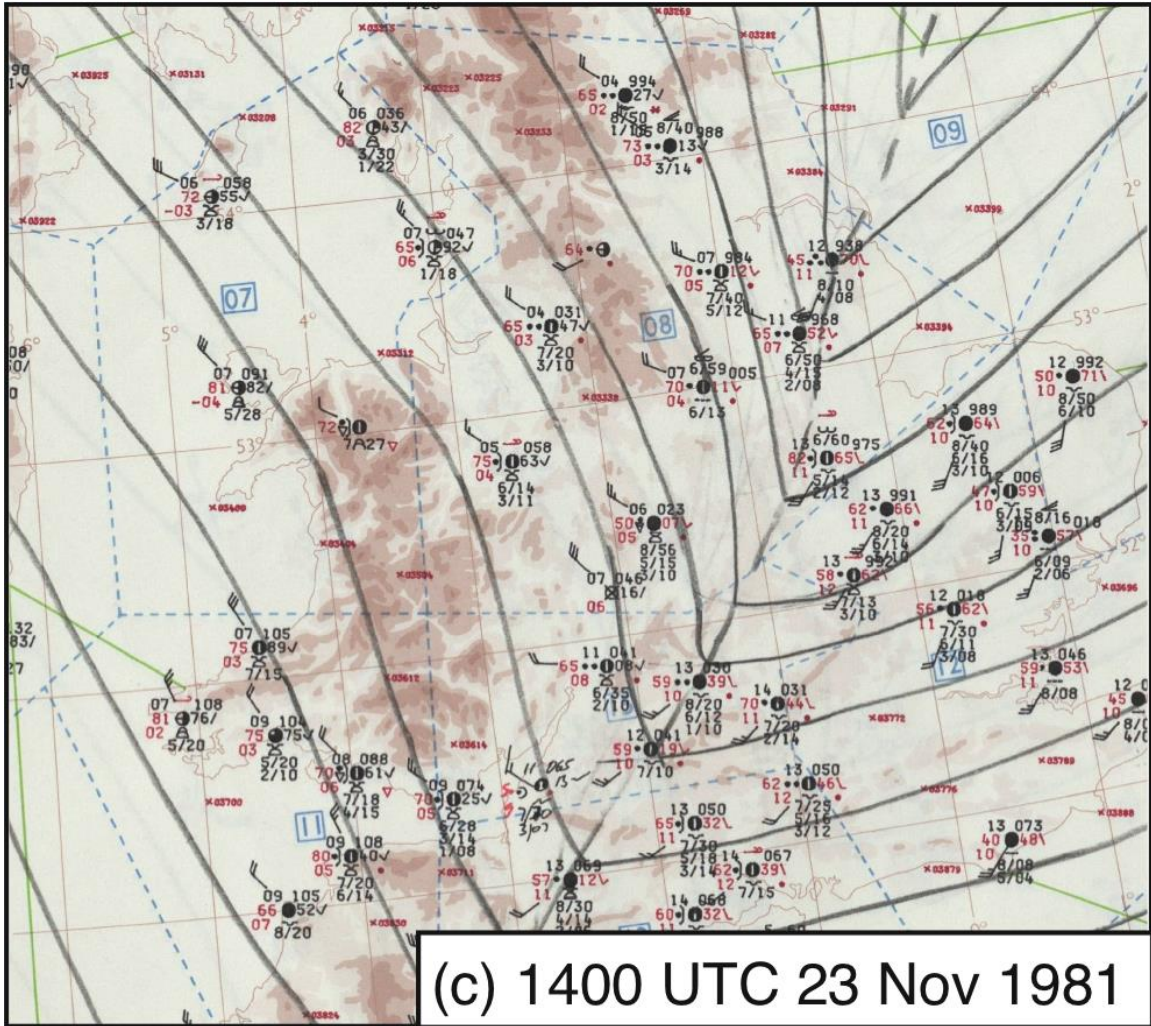
884

885



886

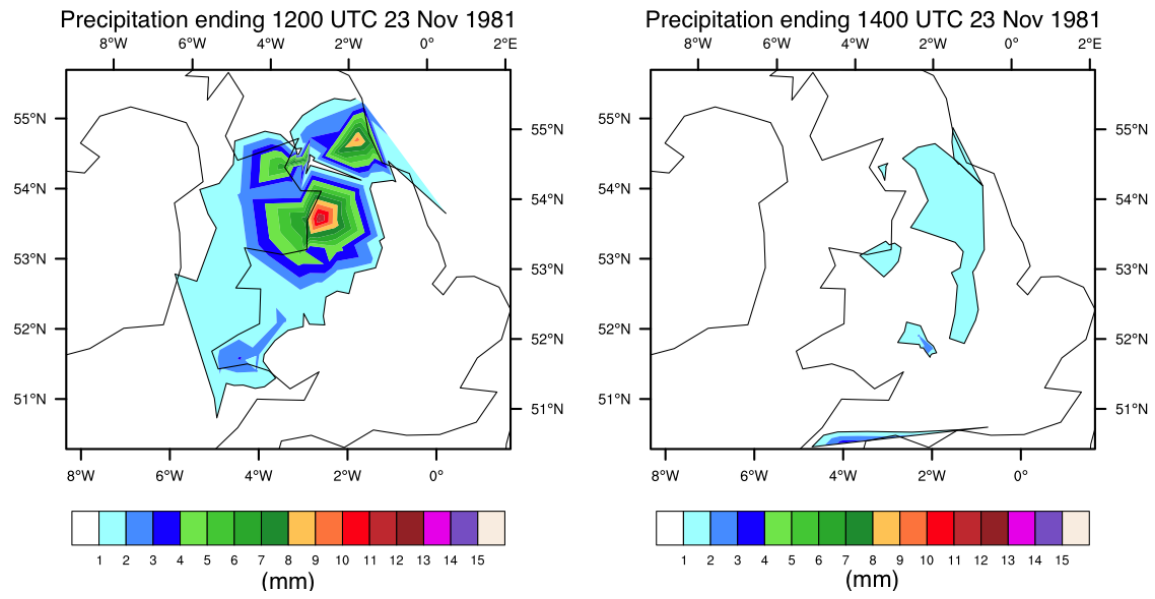
887



888

889 Figure 5. Excerpts from the Met Office Central Forecasting Office hourly U.K. working charts at
 890 (a) 1000 UTC, (b) 1200 UTC, and 1400 UTC 23 November 1981. Plotted are sea-level pressure
 891 (solid lines every 2 hPa in (a) and (c) and 4 hPa in (b)), cold front (dashed line), and standard
 892 station models. Crown copyright.

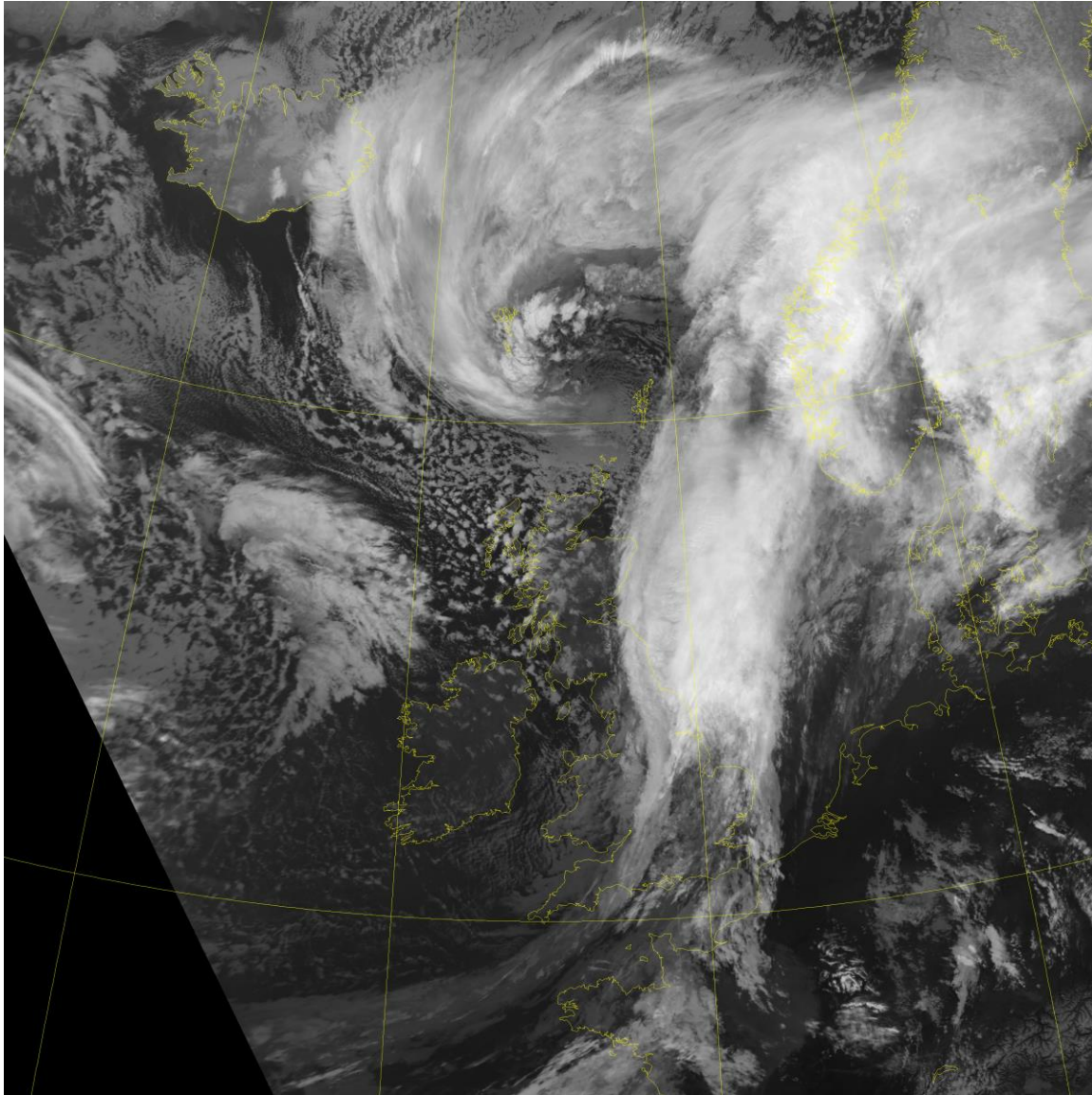
893



894

895 Figure 6. Hourly rainfall amounts (mm) from 213 rain gauges ending at 1200 UTC and 212 rain
 896 gauges ending at 1400 UTC 23 Nov 1981.

897



898

899 Figure 7. Infrared satellite imagery (channel 5, 11.5–12.5 μm) at 1325 UTC 23 Nov 1981
900 (courtesy of Dundee Satellite Receiving Station).

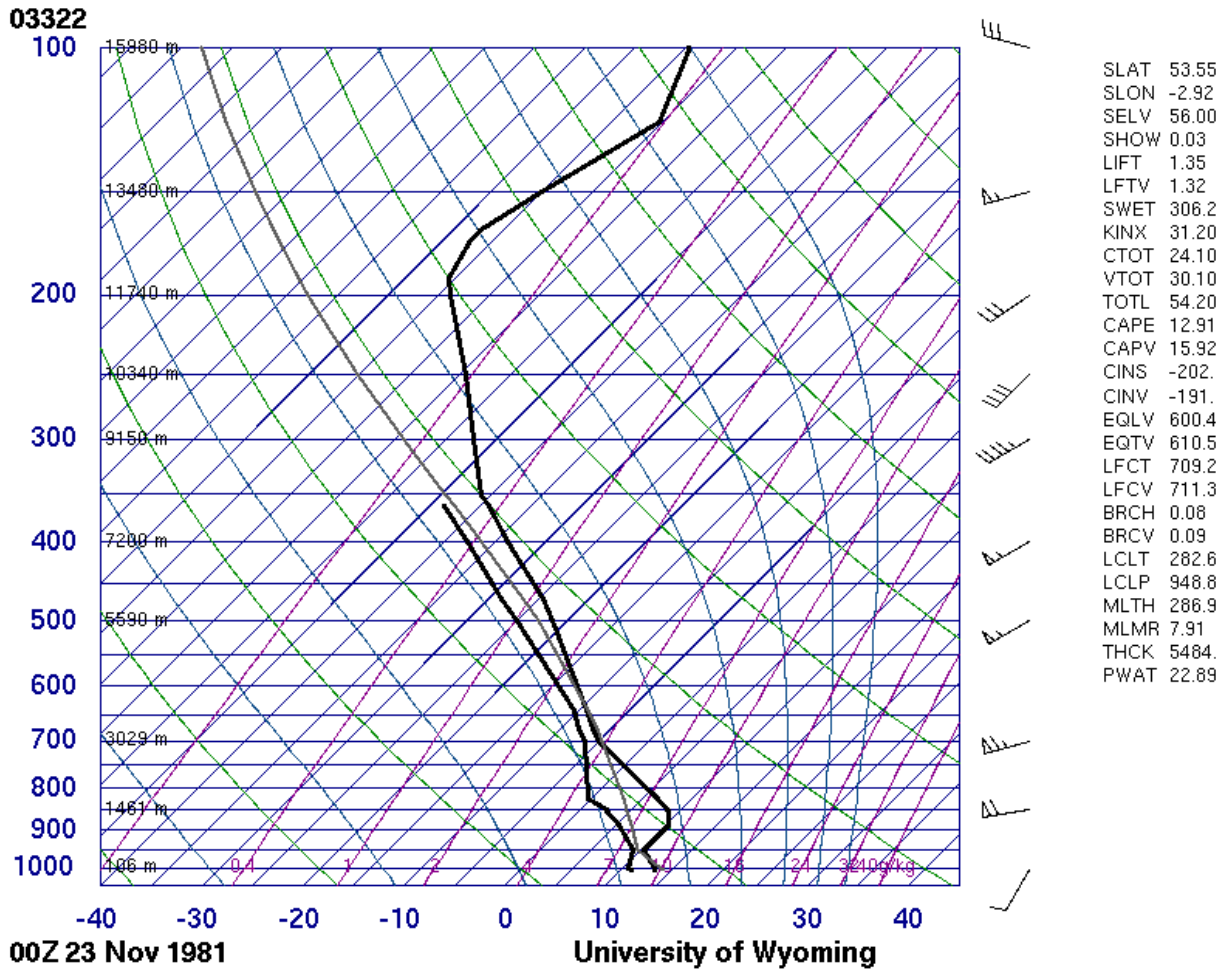
901

902

903

904

905



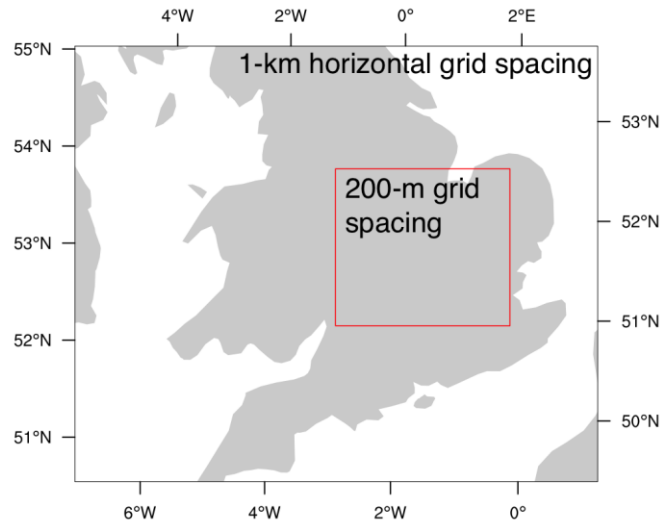
906

907

908 Figure 8. Prefrontal sounding from Aughton, near Liverpool, at 0000 UTC 23 November 1981

909 (courtesy of the University of Wyoming, <http://weather.uwyo.edu/upperair/sounding.html>).

910

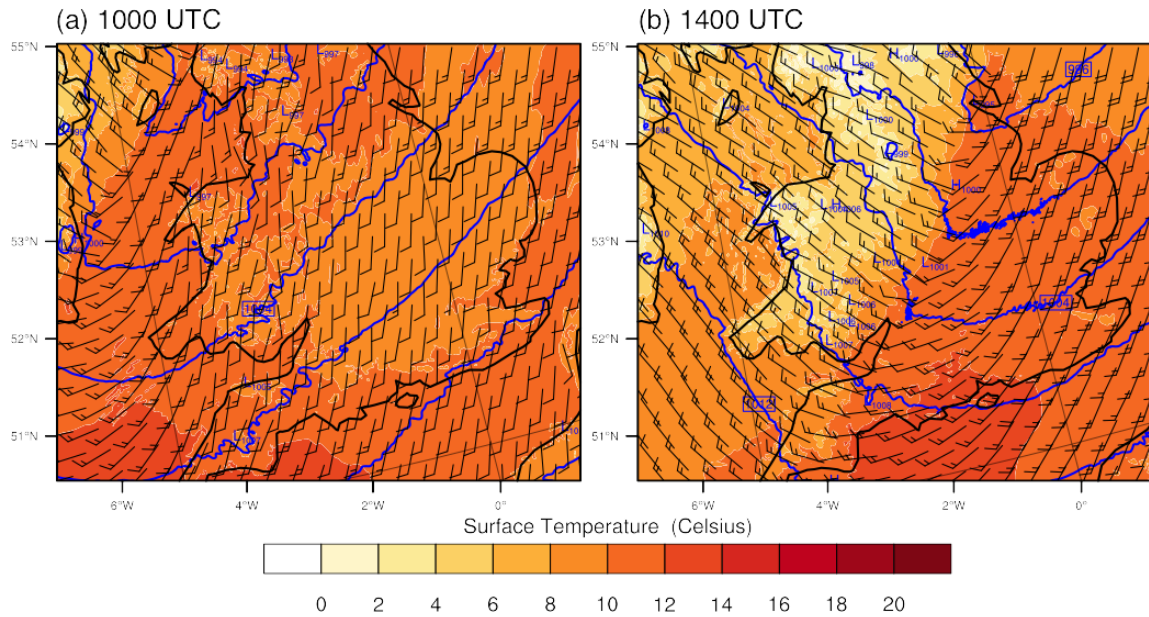


911

912 Figure 9. The two innermost domains used in this simulation.

913

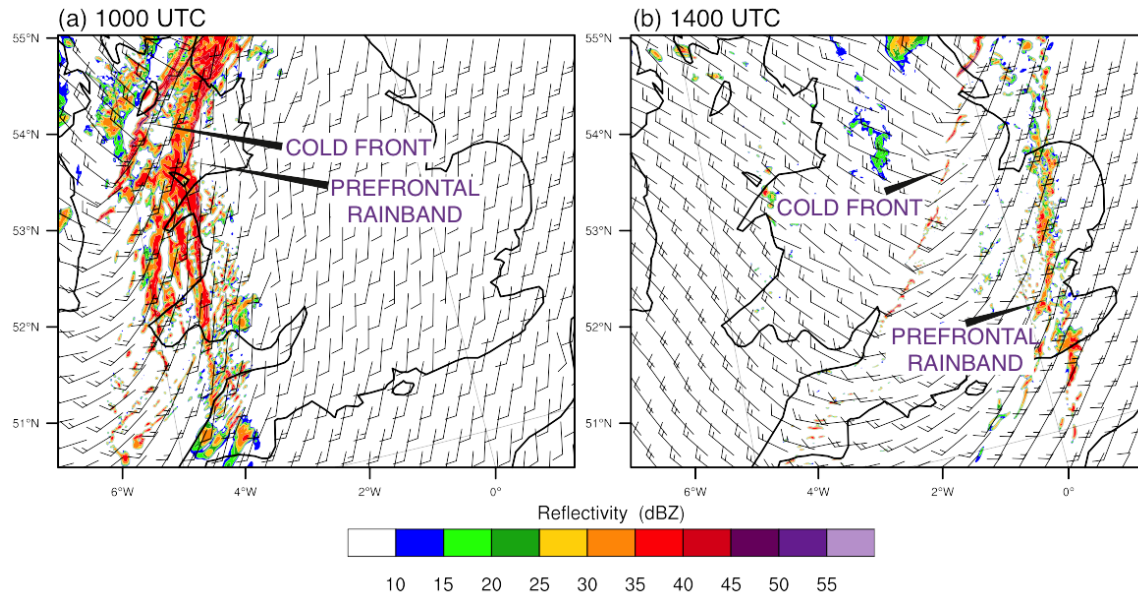
914



915

916 Figure 10. Simulation of sea level pressure (hPa, blue lines), surface temperature (°C, colored
917 according to scale), and surface winds (pennant, full barb, and half-barb denote 25, 5, 2.5 m s⁻¹,
918 respectively; separation between displayed wind vectors is 30 km) on the domain with 1-km
919 horizontal grid spacing at (a) 1000 UTC and (b) 1400 UTC 23 November 1981.

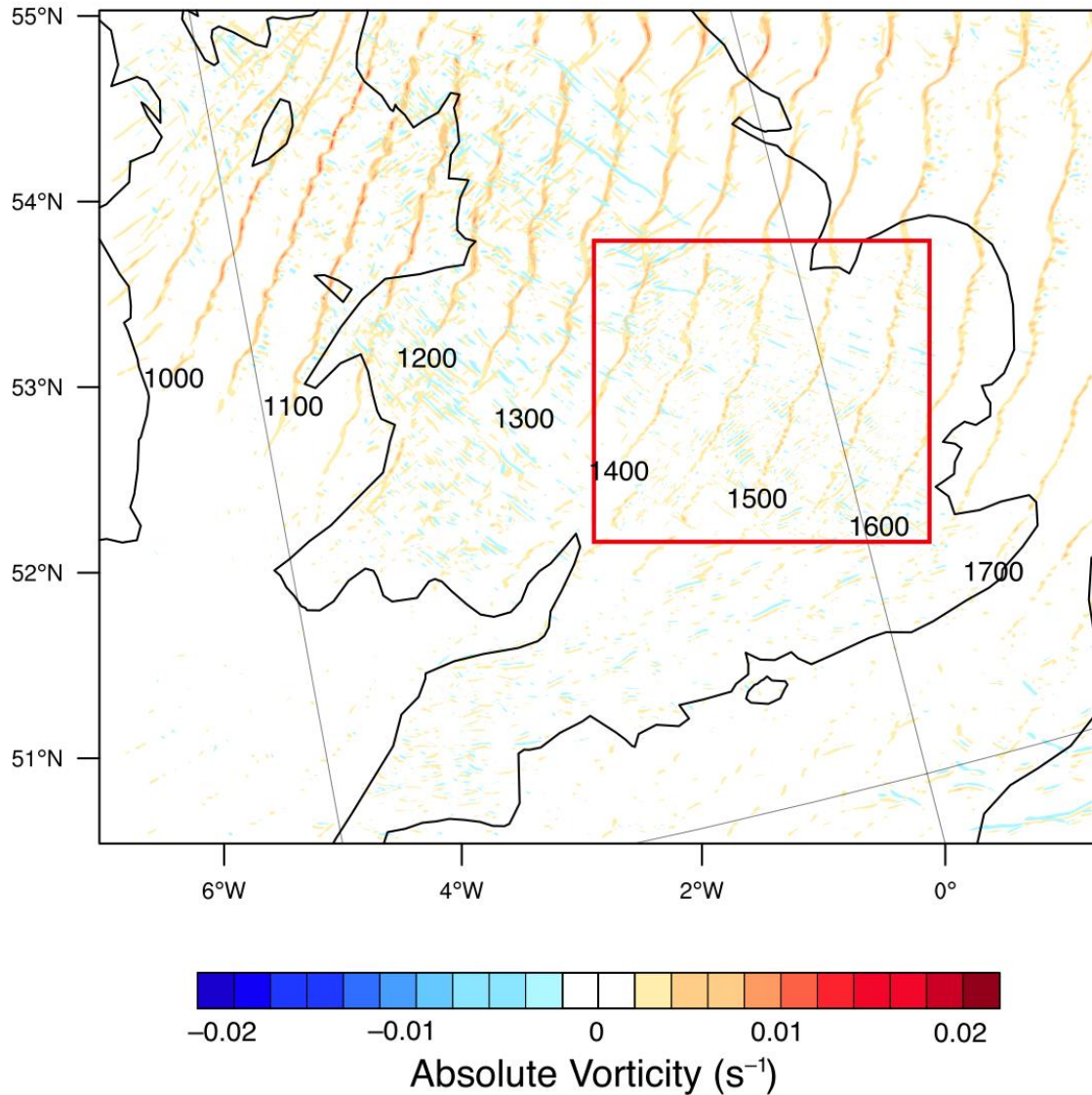
920



921

922 Figure 11. Simulation of radar reflectivity factor (dBZ, colored according to scale) and surface
 923 winds (pennant, full barb, and half-barb denote 25, 5, 2.5 m s^{-1} , respectively; separation between
 924 displayed wind vectors is 30 km) on the domain with 1-km horizontal grid spacing at (a) 1000
 925 UTC and (b) 1400 UTC 23 November 1981.

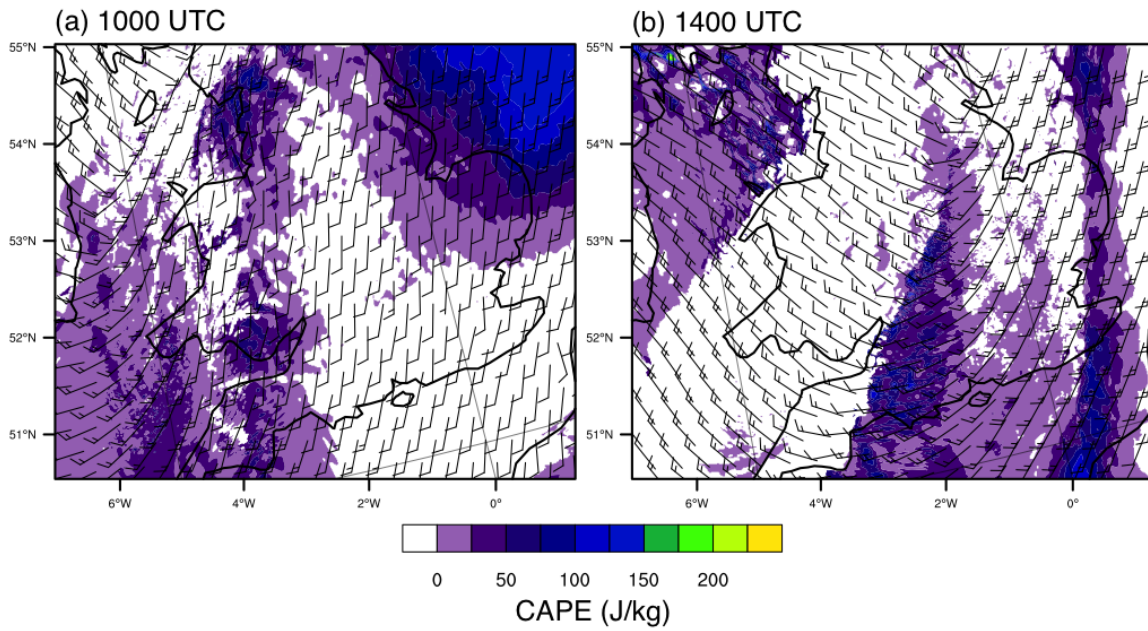
926



927

928 Figure 12. Simulation of absolute vorticity at 500 m ASL (s^{-1} , colored according to scale)
 929 every 30 min from 0930 UTC to 1730 UTC (labeled every hour) on the domain with 1-km
 930 horizontal grid spacing. The red box indicates the location of the domain with 200-m
 931 horizontal grid spacing.

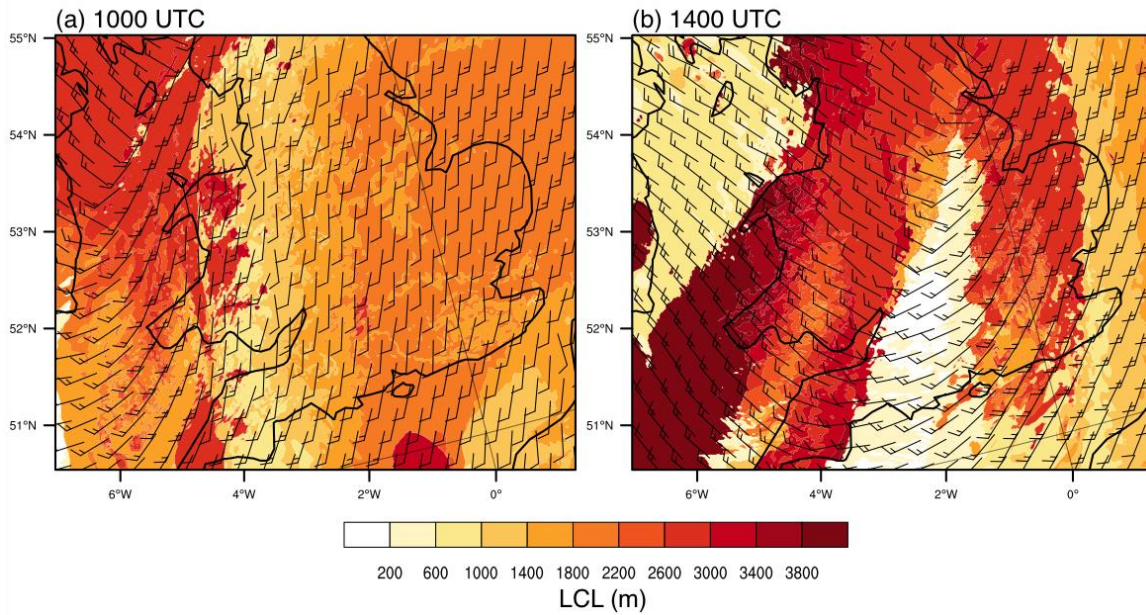
932



934

935 Figure 13. Simulation of CAPE (J kg^{-1} , colored according to scale) and surface winds
 936 (pennant, full barb, and half-barb denote 25, 5, 2.5 m s^{-1} , respectively; separation between
 937 displayed wind vectors is 30 km) on the domain with 1-km horizontal grid spacing at (a) 1000
 938 UTC and (b) 1400 UTC 23 November 1981.

939

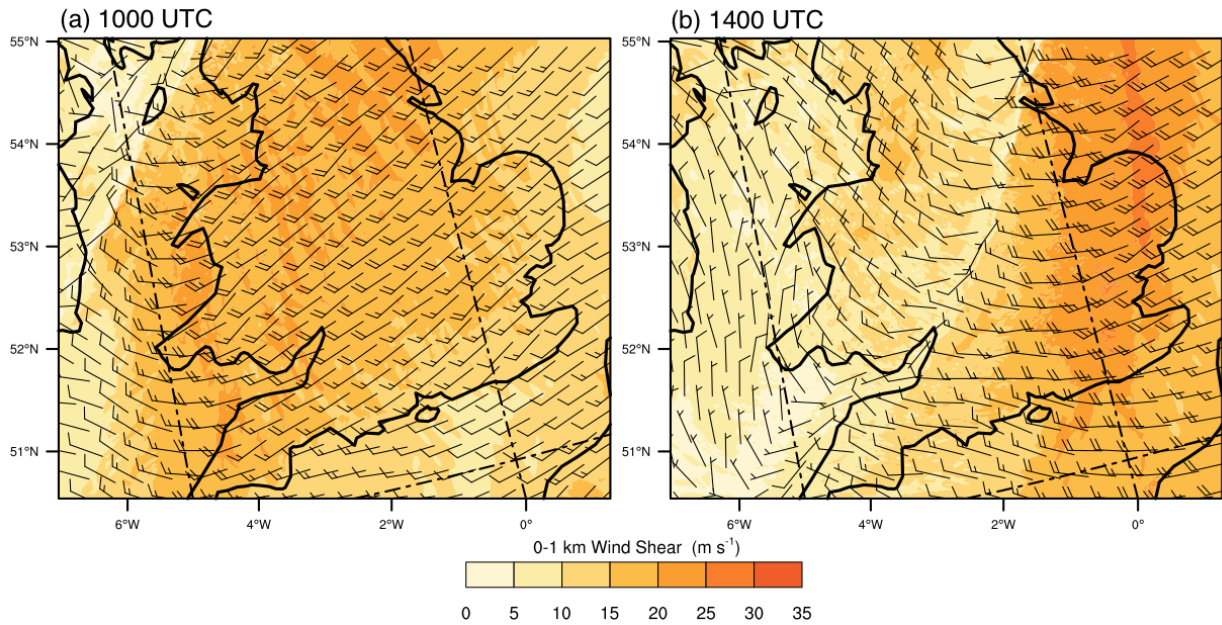


940

941 Figure 14. Simulation of lifting condensation level (LCL) (m, colored according to scale) and
 942 surface winds (pennant, full barb, and half-barb denote $25, 5, 2.5 \text{ m s}^{-1}$, respectively;
 943 separation between displayed wind vectors is 30 km) on the domain with 1-km horizontal grid
 944 spacing at (a) 1000 UTC and (b) 1400 UTC 23 November 1981.

945

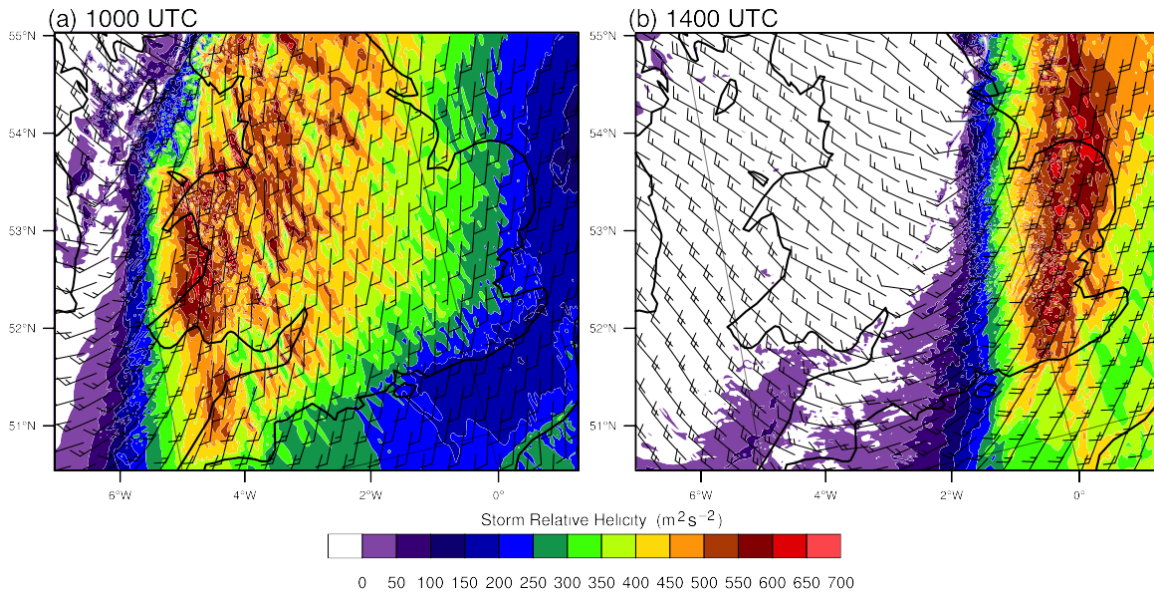
946



947

948 Figure 15. Simulation of 0–1-km vertical shear of the horizontal wind in magnitude (m s^{-1} ,
 949 colored according to scale) and direction (pennant, full barb, and half-barb denote 25, 5, 2.5 m s^{-1} ,
 950 respectively; separation between displayed wind vectors is 30 km) on the domain with 1-
 951 km horizontal grid spacing at (a) 1000 UTC and (b) 1400 UTC 23 November 1981.

952



953

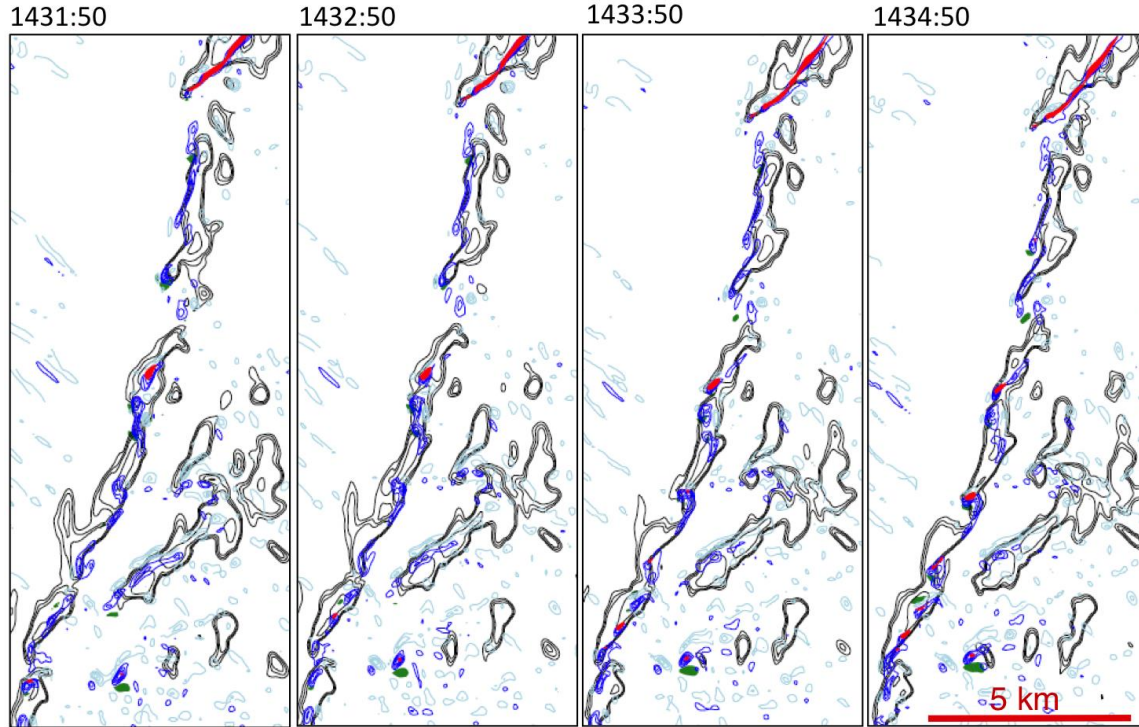
954 Figure 16. Simulation of 0–1-km storm-relative helicity ($\text{m}^2 \text{s}^{-2}$, colored according to scale)

955 and surface winds (pennant, full barb, and half-barb denote 25, 5, 2.5 m s^{-1} , respectively;

956 separation between displayed wind vectors is 30 km) on the domain with 1-km horizontal grid

957 spacing at (a) 1000 UTC and (b) 1400 UTC 23 November 1981.

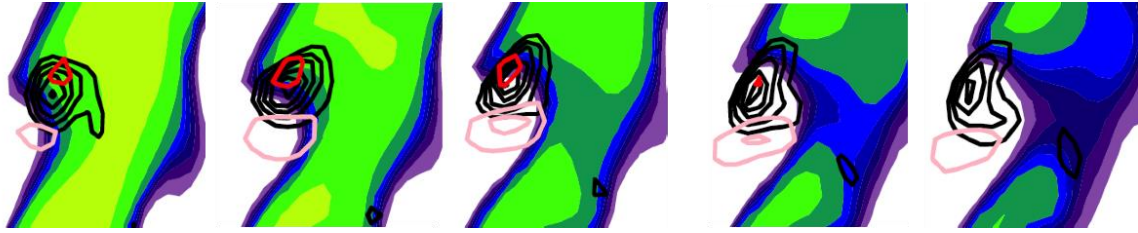
958



959

960 Figure 17. Simulation of radar reflectivity factor (black lines every 10 dBZ), absolute vorticity at
 961 500 m ASL (positive values are contoured in dark blue solid lines every 0.005 s^{-1} , starting from
 962 0.01 s^{-1} ; negative values are contoured in light blue solid lines every -0.005 s^{-1} every 0.005 s^{-1}),
 963 500-m updrafts (red fill above 5 m s^{-1}), and 500-m downdrafts (green fill above 2 m s^{-1}) from the
 964 200-m horizontal grid spacing domain, plotted every minute from 1431:50 to 1434:50 UTC 23
 965 November 1981.

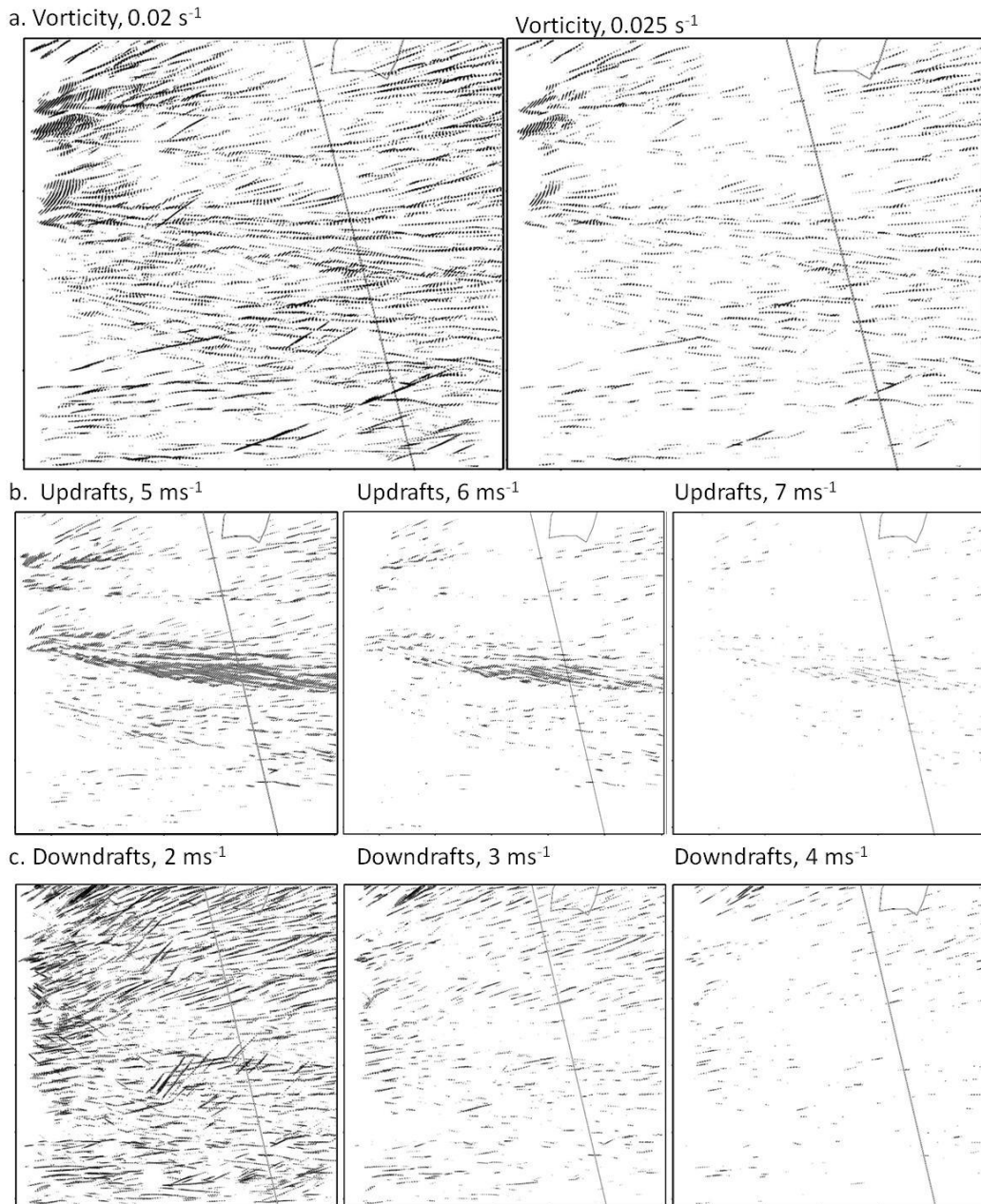
966



967

968 Figure 18. Characteristic structure and evolution of a simulated misovortex within the domain at
 969 200-m horizontal grid spacing, plotted every 60 s around the time that it matures: radar
 970 reflectivity factor (dBZ, colored according to scale in Fig. 16), absolute vorticity at 500 m ASL
 971 (black contours every 0.005 s^{-1} , starting from 0.01 s^{-1}), 500-m updraft (red contours every 5 m s^{-1})
 972 1), and 500-m downdraft (pink contours every 2 m s^{-1}). Each panel is about $4 \text{ km} \times 4 \text{ km}$, and
 973 the vortex is about 500 m across.

974



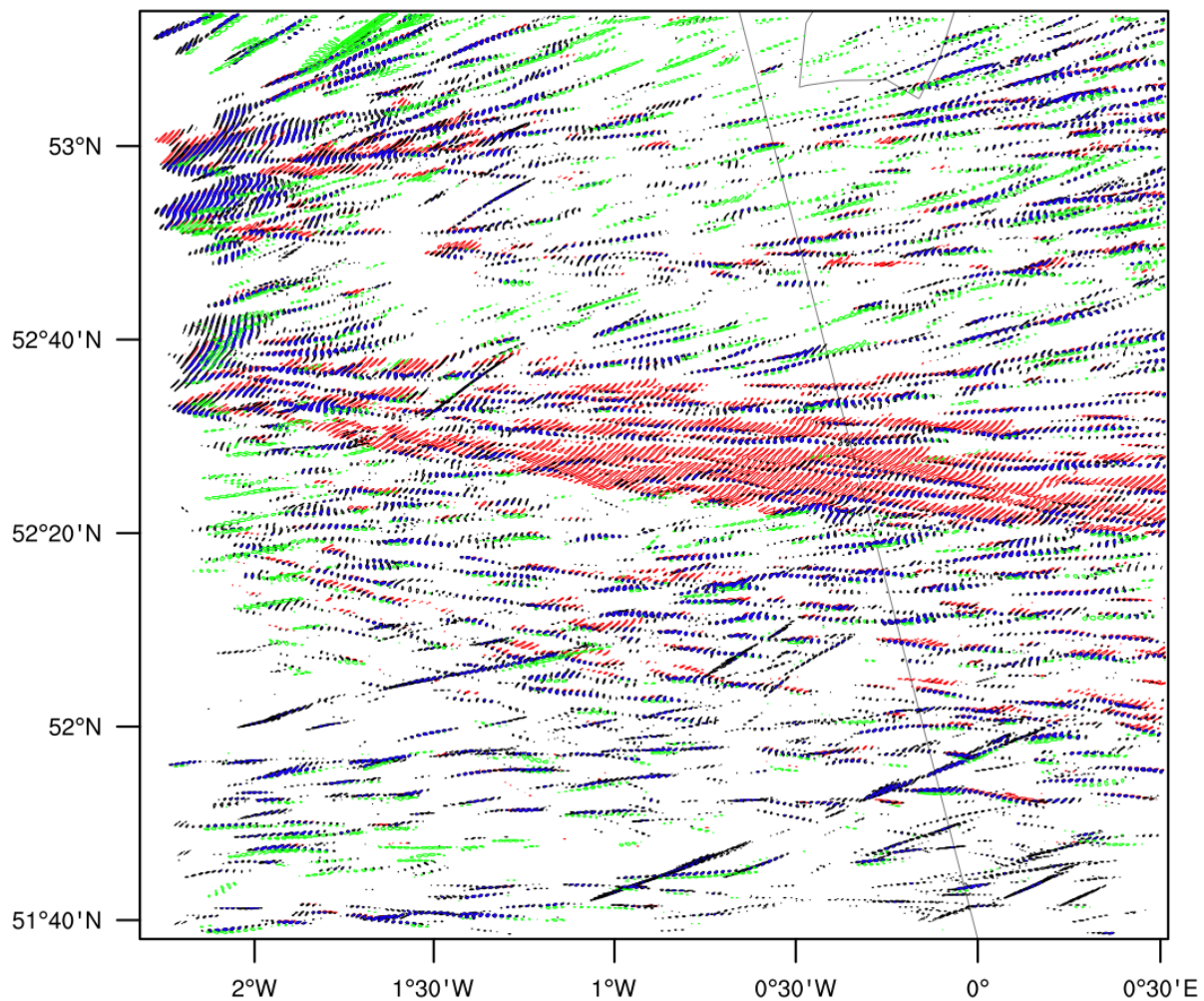
986

987 Figure 20. Tracks of (a) 500-m absolute vorticity (0.02 and 0.025 s^{-1}), (b) 500-m updrafts (5,

988 6, and 7 m s^{-1}), and (c) 500-m downdrafts (2 , 3 , and 4 m s^{-1}) plotted every minute from 1300

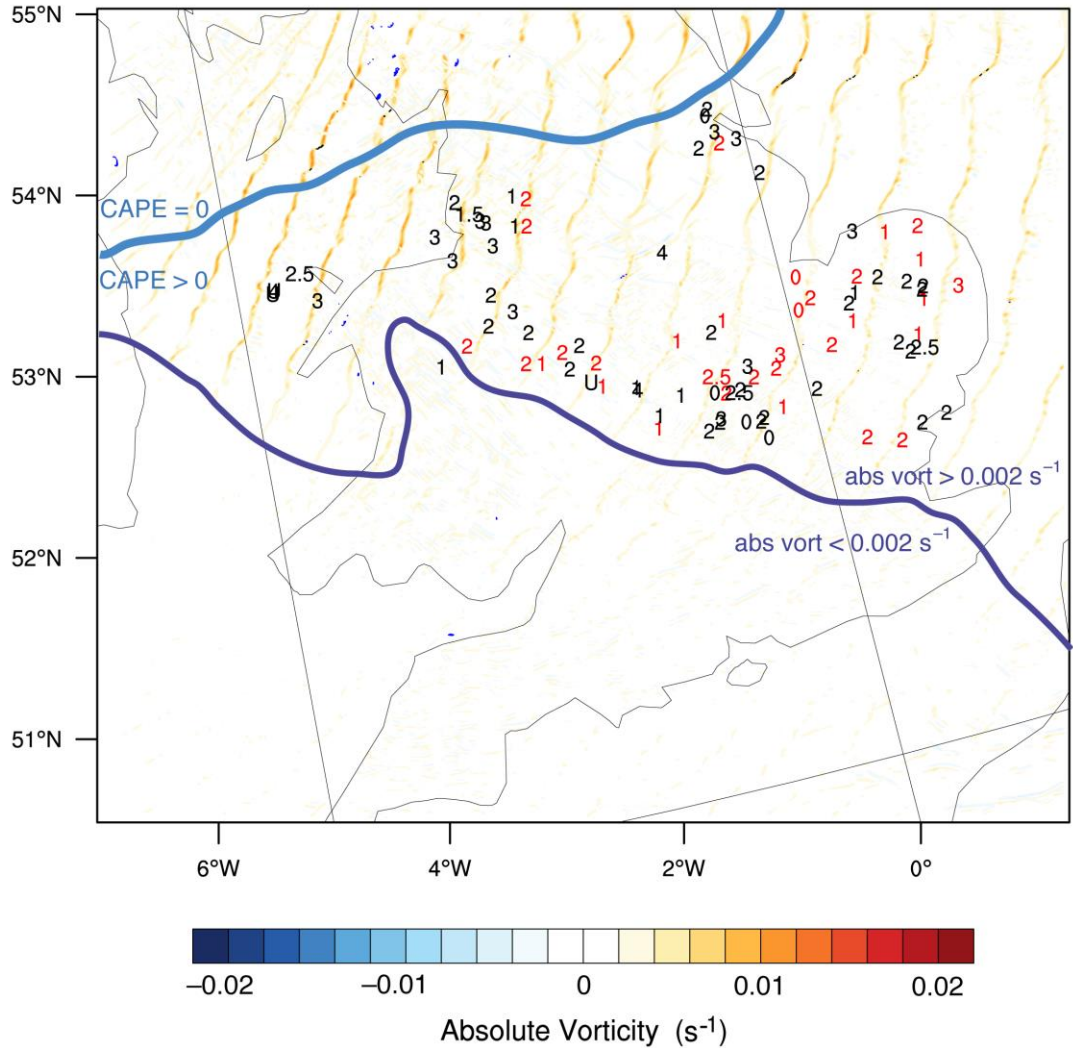
989 to 1600 UTC in the domain with 200-m horizontal grid spacing.

990



991
 992 Figure 21. Simulation of 0.02 s^{-1} and 0.025 s^{-1} absolute vorticity at 500 m ASL (black
 993 contours), 5 m s^{-1} updrafts at 500 m (red contours), and 3 m s^{-1} downdrafts at 500 m (green
 994 contours) from 1300 to 1600 UTC on the domain with 200-m horizontal grid spacing.

995



996

997 Figure 22. Simulation of absolute vorticity at 500 m ASL (s^{-1} , colored according to scale)
 998 every 30 min from 0930 UTC to 1730 UTC on the domain with 1-km horizontal grid spacing.
 999 Purple lines separate approximate areas with simulated absolute vorticity less than $0.002 s^{-1}$
 1000 on the 1-km domain during the time of frontal passage. Blue lines separate approximate areas
 1001 with simulated positive CAPE during the time of frontal passage. Locations of reports that
 1002 appear to be located over water are a result of a coarse representation of geography. Locations
 1003 of the 90 tornado reports from the TORRO database for 23 November 1981. Numbers
 1004 represent their strength on the T scale. Reports verified by TORRO (58) are classified as
 1005 definite and plotted in black. Reports that have not been verified (32) are classified as
 1006 probable and are plotted in red.